

10-7-2011

Exploiting the Power Law Distribution Properties of Satellite Fire Radiative Power Retrievals: A Method to Estimate Fire Radiative Energy and Biomass Burned from Sparse Satellite Observations

S. S. Kumar

South Dakota State University

David P. Roy

South Dakota State University, david.roy@sdstate.edu


L. Boschetti

University of Maryland College Park

R. Kremens

Rochester Institute of Technology

Follow this and additional works at: https://openprairie.sdstate.edu/gsce_pubs

 Part of the [Physical and Environmental Geography Commons](#), [Remote Sensing Commons](#), and the [Spatial Science Commons](#)

Recommended Citation

Kumar, S. S., D. P. Roy, L. Boschetti, and R. Kremens (2011), Exploiting the power law distribution properties of satellite fire radiative power retrievals: A method to estimate fire radiative energy and biomass burned from sparse satellite observations, *J. Geophys. Res.*, 116, D19303, doi:10.1029/2011JD015676.

This Article is brought to you for free and open access by the Geospatial Sciences Center of Excellence (GSCE) at Open PRAIRIE: Open Public Research Access Institutional Repository and Information Exchange. It has been accepted for inclusion in GSCE Faculty Publications by an authorized administrator of Open PRAIRIE: Open Public Research Access Institutional Repository and Information Exchange. For more information, please contact michael.biondo@sdstate.edu.

Exploiting the power law distribution properties of satellite fire radiative power retrievals: A method to estimate fire radiative energy and biomass burned from sparse satellite observations

S. S. Kumar,¹ D. P. Roy,¹ L. Boschetti,² and R. Kremens³

Received 21 January 2011; revised 18 July 2011; accepted 23 July 2011; published 7 October 2011.

[1] Instantaneous estimates of the power released by fire (fire radiative power, FRP) are available with satellite active fire detection products. The temporal integral of FRP provides an estimate of the fire radiative energy (FRE) that is related linearly to the amount of biomass burned needed by the atmospheric emissions modeling community. The FRE, however, is sensitive to satellite temporal and spatial FRP undersampling due to infrequent satellite overpasses, cloud and smoke obscuration, and failure to detect cool and/or small fires. Satellite FRPs derived over individual burned areas and fires have been observed to exhibit power law distributions. This property is exploited to develop a new way to derive FRE, as the product of the fire duration and the expected FRP value derived from the FRP power law probability distribution function. The method is demonstrated and validated by the use of FRP data measured with a dual-band radiometer over prescribed fires in the United States and by the use of FRP data retrieved from moderate resolution imaging spectroradiometer (MODIS) active-fire detections over Brazilian deforestation and Australian savanna fires. The biomass burned derived using the conventional FRP temporal integration and power law FRE estimation methods is compared with biomass burned measurements (prescribed fires) and available fuel load information reported in the literature (Australian and Brazilian fires). The results indicate that the FRE power law derivation method may provide more reliable burned biomass estimates under sparse satellite FRP sampling conditions and correct for satellite active-fire detection omission errors if the FRP power law distribution parameters and the fire duration are known.

Citation: Kumar, S. S., D. P. Roy, L. Boschetti, and R. Kremens (2011), Exploiting the power law distribution properties of satellite fire radiative power retrievals: A method to estimate fire radiative energy and biomass burned from sparse satellite observations, *J. Geophys. Res.*, 116, D19303, doi:10.1029/2011JD015676.

1. Introduction

[2] Spatially and temporally explicit mapping of the amount of biomass burned by fire is needed to estimate atmospheric emissions of greenhouse gases and aerosols that have a significant climate-forcing effect [Crutzen and Andreae, 1990; Denman *et al.*, 2007]. Satellite data have been used to monitor fire for more than two decades using algorithms that detect the location of fires actively burning at the time of satellite overpass, and in the past few decades using burned area mapping algorithms that map the spatial extent of the areas affected by fires [Robinson, 1991; Fredericksen *et al.*, 1990; Fuller, 2000; Chuvieco and Martin, 1994; Giglio *et al.*, 2003; Roy *et al.*, 2008]. Recently,

researchers have been attempting to use satellite data to characterize active-fire properties, including parameters related to the intensity of the fire [Lentile *et al.*, 2006]. The instantaneous fire radiative power (FRP) (units: W) is retrieved at active-fire detections from mid-infrared wavelength remotely sensed data and can be used to estimate the rate of biomass consumed [Kaufman *et al.*, 1996, 1998]. Temporal integration of continuously sampled FRP over the duration of the fire provides the fire radiative energy (FRE) (units: J), which has been shown, with both laboratory and field measurements, to be linearly related to the total biomass burned (units: g) [Wooster *et al.*, 2005; Freeborn *et al.*, 2008]. This approach provides the opportunity to map biomass burned from space without the need for fuel load and combustion completeness information that are not reliably defined at regional to global scales [Robinson, 1989; Korontzi *et al.*, 2004; van der Werf *et al.*, 2006; Ellicott *et al.*, 2009; Vermote *et al.*, 2009]. However, the retrieval of the FRE, and thus of the biomass burned, is sensitive to satellite spatial and temporal sampling of FRP [Boschetti and Roy, 2009; Freeborn *et al.*, 2011]. This paper seeks to

¹Geographic Information Science Center of Excellence, South Dakota State University, Brookings, South Dakota, USA.

²Department of Geography, University of Maryland, College Park, Maryland, USA.

³Center for Imaging Science, Rochester Institute of Technology, Rochester, New York, USA.

develop a methodology to derive FRE that is less sensitive to FRP-sampling issues.

[3] Recent research indicates that satellite FRP retrievals over individual burned areas and fires have power law distributions [Wooster and Zhang, 2004; Roberts et al., 2005; Roberts and Wooster, 2008]. Power law distributions are observed across other natural phenomena, including fire sizes [Malamud et al., 2005; Corral et al., 2008; Lin and Rinaldi, 2009; Zinck et al., 2010], fire return intervals [Song et al., 2006], the magnitude of earthquakes and the size of lunar craters [Newman, 2005], lake sizes [Downing et al., 2006; Zhang et al., 2009], and cloud sizes [Koren et al., 2008]. In this paper, the mathematical properties of power law distributions are used to develop an alternative method to estimate FRE that we show, under certain conditions, may be less sensitive to satellite FRP sampling issues compared with the conventional time integral of FRP. We consider the power law properties of FRP measurements made with a dual-band radiometer for eight prescribed fires in the United States and use FRP retrieved from the moderate-resolution imaging spectroradiometer (MODIS) Terra and Aqua satellites over Australian savanna fires and Brazilian deforestation fires that have contrasting fuel loads and burning conditions. The FRE derived biomass burned estimates for the power law and conventional FRE estimation methods are compared with the measured total fuel consumed (U.S. prescribed fires) and with available fuel load information reported in the literature (Australian and Brazilian fires).

[4] Using a priori knowledge about the power law distribution of FRP, we show that we can compensate for the lack of information on the temporal evolution of FRP retrieved from polar-orbiting satellite observations due to satellite undersampling of FRP and also compensate for decreased probability of satellite detection of fires with low FRP. We show that the FRE can be estimated as the product of the expected FRP derived from three FRP power law distribution parameters and the fire duration. Sensitivity analyses with respect to these parameters are reported. If the FRP power law distribution parameters are reasonably well constrained, then the uncertainties in FRE estimates are reduced to the uncertainties in the estimation of the fire duration only. Under these circumstances, the power law based FRE estimates are shown to provide more accurate results than conventional FRP temporal integration approaches.

2. Theoretical Considerations

2.1. FRP and FRE

[5] The total FRE (units: J) released by a fire is defined, for the ideal case of continuous measurement of FRP (units: W), as follows:

$$FRE = \int_{t=0}^{t=d} FRP(t)dt, \quad (1)$$

where d is the duration (units: s) of the fire. In the case of discrete measurements of FRP, the FRE can be estimated using the trapezoid numerical integration method, with the implicit assumption that there is sufficient temporal FRP

sampling and a linear change of FRP between successive FRP measurements [Boschetti and Roy, 2009], as follows:

$$FRE_{num.int} \approx \sum_{i=1}^{i=n} \frac{(t_{i+1} - t_i)(FRP_{i+1} + FRP_i)}{2}, \quad (2)$$

where t_i is the time FRP_i is measured and n is the number of FRP measurements over the duration of the fire. If the discrete measurements are made equally spaced in time, then equation (2) can be expressed as

$$FRE \approx d \sum_{i=1}^{i=n} \frac{FRP_i}{n}, \quad (3)$$

where d is the duration of fire, expressed as $d = n\Delta t$, if Δt is the time interval between successive FRP measurements. In the limit of an infinite number of measurements, the summation term in (3) is the expected/expectation FRP value and the FRE can be defined as

$$FRE = d\langle FRP \rangle, \quad (4)$$

where $\langle FRP \rangle$ is the expected FRP value over the fire duration d (units: s). We note that, for a small number of FRP samples, the arithmetic mean and the expected FRP values can be quite different.

[6] It is established that fires have temporal fluctuations in fire radiant power and so the FRE estimated by numerical integration of FRP measurements is sensitive to satellite FRP undersampling [Boschetti and Roy, 2009]. Satellite data provide the only way to monitor fires over large geographic areas. However, active-fire detections from polar-orbiting satellites undersample the temporal variability of fires because of the long intervals between consecutive satellite overpasses [Giglio, 2007], and they also undersample the spatial extent of the area affected by the fire if the fire progresses rapidly across the landscape [Roy et al., 2008]. Geostationary satellites provide improved temporal sampling compared with polar-orbiting systems, but they typically have lower spatial resolution that can effect FRP estimation. For example, Roberts and Wooster [2008] reported that geostationary SEVIRI data underestimated regional-scale total FRP by 40% to 50% compared with MODIS because of the SEVIRI non-detection of many low-intensity fire pixels (FRP < 50 MW). The retrieval of FRP from satellite data may also be sensitive to factors including the subpixel location of the fire and the sensing system point spread function, the fire background characterization used in the FRP retrieval algorithm, and the presence of atmospheric water vapor [Wooster et al., 2005; Calle et al., 2009; Schroeder et al., 2010]. Furthermore as with all satellite sensing systems, fires are obscured by clouds, smoke, and optically thick aerosols [Roy et al., 2008].

[7] If the temporal probability distribution of FRP can be characterized, then this information may be used to help provide more reliable FRE estimates under sparse satellite FRP-sampling conditions. Regional to continental scale satellite studies have shown that the mean FRP extracted over large geographic areas exhibits a diurnal temporal variability that has been parameterized using modified Gaussian functions of FRP against time [Roberts and Wooster, 2008; Ellicott et al., 2009; Vermote et al., 2009].

At the scale of individual burned areas and fires, however, the temporal evolution of FRP does not exhibit a smooth or Gaussian temporal variability [Wooster *et al.*, 2005; Roberts and Wooster, 2008]. This is because of local variation in the prefire fuel load and fire behavior. For example, the FRP of grassland fires has been observed to change by an order of magnitude with fluctuations in the wind direction relative to the unburned fuel bed [Smith and Wooster, 2005]. Recent research indicates that satellite FRP retrievals over individual burned areas and fires exhibit power law distributions [Wooster and Zhang, 2004; Roberts *et al.*, 2005; Roberts and Wooster, 2008], and so this property may enable reliable FRE estimates under sparse satellite FRP temporal sampling conditions, such as provided by polar-orbiting satellites and/or remote sensing under cloudy and thick-smoke conditions.

2.2. Exploiting the Power Law Properties of FRP Temporal Variability

[8] Power law distributions have probability distribution functions of the following form:

$$P(x) = c x^{-m}, \quad (5)$$

where $P(x)$ is the probability distribution function of a continuous real variable x , c is a constant, and m is a scaling parameter [Newman, 2005]. For power law distributed data the arithmetic mean of a set of samples provides an unreliable estimate of the expected value, especially when the set of samples is small [Newman, 2005].

[9] The expected value of a power law distribution can be derived analytically. First, the probability distribution is normalized by evaluating the integral of $P(x)$ over all values and setting this to one so that the constant c becomes

$$c = (1 - m) \left(\frac{1}{x_{\max}^{-m+1} - x_{\min}^{-m+1}} \right). \quad (6)$$

[10] The expected value $\langle x \rangle$ is then defined as follows:

$$\begin{aligned} \langle x \rangle &= \int_{x_{\min}}^{x_{\max}} P(x)x dx = \int_{x_{\min}}^{x_{\max}} c x^{-m+1} dx \\ &= (1 - m) \left(\frac{1}{x_{\max}^{-m+1} - x_{\min}^{-m+1}} \right) \left(\frac{x_{\max}^{(-m+2)} - x_{\min}^{(-m+2)}}{(2 - m)} \right), \end{aligned} \quad (7)$$

where x_{\min} and x_{\max} are the lower and upper limit of the range of possible x values and m is a scaling parameter [Newman, 2005].

[11] Assuming that the FRP over the duration of the fire follows a power law distribution, then the FRE can be estimated by substituting FRP for x in (7) and combining with (4), as follows:

$$\begin{aligned} FRE_{\text{pwr law}} = d \langle FRP \rangle &= d(1 - m) \left(\frac{1}{FRP_{\max}^{(-m+1)} - FRP_{\min}^{(-m+1)}} \right) \\ &\cdot \left(\frac{FRP_{\max}^{(-m+2)} - FRP_{\min}^{(-m+2)}}{(2 - m)} \right), \end{aligned} \quad (8)$$

where d is the duration of the fire, m is the scaling parameter of the power law distribution, and FRP_{\min} and FRP_{\max} are the minimum and maximum possible FRP values. This formulation provides an alternate way to estimate the FRE from conventional numerical integration methods, such as (2). We note, however, that (8) is indeterminate or evaluates to zero depending on specific values of m , FRP_{\min} , and FRP_{\max} . Specifically, $FRE_{\text{pwr law}}$ will evaluate to zero for $m = 1$, is indeterminate for $m = 2$, and will be sensitive to FRP_{\min} and FRP_{\max} when $m < 2$. We also note that the minimum and maximum possible FRP values are unknown; for this study, we set FRP_{\min} and FRP_{\max} as the minimum and maximum observed FRP values, respectively. A sensitivity analysis to the choice of FRP_{\min} and FRP_{\max} is presented in section 5.3 for the cases when $m > 2$ and $m < 2$.

2.3. Fitting a Power Law Distribution to Discrete Empirical Data

[12] The scaling parameter m can be estimated from discrete measurements by the use of a number of empirical methods. The three primary methods are the maximum likelihood estimator (MLE), the linear regression fit to cumulative-probability distribution function in log scales (LR+CDF), and the linear regression fit to probability distribution function in log scales (LR+PDF) [Goldstein *et al.*, 2004; Newman, 2005; Clauset *et al.*, 2009]. The LR+PDF method is the simplest method, requires no a priori assumptions, and so is frequently used [Malamud *et al.*, 2005; Downing *et al.*, 2006; Song *et al.*, 2006; Koren *et al.*, 2008; Zhang *et al.*, 2009].

[13] In this paper, the LR+PDF method is adapted following suggestions by [Newman, 2005] to address issues concerning errors that may occur in the regression computation. The probability distribution function (5) of a discrete set of measurements of x is defined by the histogram of x and is linearized by taking the natural logarithm of the distribution function as follows:

$$\ln|P(x_i)| = \ln|c| - m \ln|x_i|, \quad (9)$$

where the range of the variable x is partitioned in n discrete bins (intervals), x_i is the central point of each bin with $i \in \{1 \dots n\}$, and $P(x_i)$ is the probability of a value x falling in the i th bin. The coefficient $\ln|c|$ and the scaling parameter m are estimated by a linear regression with $\ln|P(x_i)|$ and $\ln|x_i|$ as the response and predictor variables, respectively. For power law distributions, the bins that count the occurrences of large values may have more influence on the regression owing to their relatively lower counts compared with the counts in smaller-value bins [Goldstein *et al.*, 2004; Newman, 2005]. To mitigate for this effect, Newman [2005] suggested using bins with logarithmically increasing bin widths and rescaling the counts by the corresponding bin widths. In this way, we use bin intervals defined as follows:

$$\text{Interval}_i = \left(\frac{(2^{i-1} - 1)}{(2^n - 1)} x_{\max}, \frac{(2^i - 1)}{(2^n - 1)} x_{\max} \right) \quad (10)$$

and the width of the i th bin is

$$\text{Width}_i = \frac{(2^{i-1})}{(2^n - 1)} x_{\max}, \quad (11)$$

Table 1. Physical Characteristics of the Eight U.S. Prescribed Fires

Fire	Prefire Dry Litter Fuel Load (kg m ⁻²)	Prefire Woody Fuel Load (kg m ⁻²)	Prefire Total Fuel Load (kg m ⁻²)	Consumed Litter (kg m ⁻²)	Consumed Woody (kg m ⁻²)	Total Biomass Consumed (kg m ⁻²)	Number of FRP Measurements	Fire Duration (s)	FRP _{min} (W m ⁻²)	FRP _{max} (W m ⁻²)
1	0.64	1.28	1.93	0.31	0.1	0.41	68	670	6.5	12,245
2	0.31	0	0.31	0.31	0	0.31	35	340	7	12,752
3	0.16	0	0.16	0.16	0	0.16	35	340	10.7	3,786
4	0.31	0	0.31	0.31	0	0.31	27	260	30.6	20,029
5	0.92	1.26	2.18	0.84	0.73	1.57	202	2,100	6.8	12,514
6	0.63	2.17	2.8	0.63	1.49	2.12	253	2,520	6.9	10,853
7	0.95	2.2	3.15	0.95	2.2	3.15	243	2,420	13	17,870
8	0.96	2.48	3.43	0.96	2.41	3.36	251	2,500	37	20,887

where n is the total number of bins, $i \in \{1 \dots n\}$, and x_{\max} is the maximum measured x value. The binning scheme defined by (10) and (11) requires that x is always positive; this is always the case with FRP. The probability of x falling in the i th bin is as follows:

$$P(x_i) = \frac{\text{counts}_i}{q \text{ width}_i} \quad (12)$$

where counts_i is the number of observations falling in the i th bin and q is the total number of observations over all the bins. It follows that $\sum_{i=1}^n P(x_i) \text{ width}_i = 1$.

[14] In this study, the Theil-Sen nonparametric regression estimator is applied to (9) to estimate m and $\ln|c|$. The

Theil-Sen estimator is used because it is robust to outliers and, unlike ordinary least squares regression estimators, makes only weak assumptions about the probability distribution of the response and predictor errors [Theil, 1950; Sen, 1968; Fernandes and Leblanc, 2005]. For certain bins, $P(x_i)$ may be zero; these bins are ignored in the application of the regression. The correlation (r) between the predicted and observed values is derived as an indicator of the regression goodness of fit. The scaling parameter m is sensitive to the number of bins n . However, because there is no analytical solution for an optimal n , we use an iterative method, where n is increased monotonically from a starting value of 5, up to a maximum of 100 (which was adequate to fit a power law for the data sets used in this study). In each iteration, if at least 5 bins have non-zero sample counts, the Theil-Sen regression

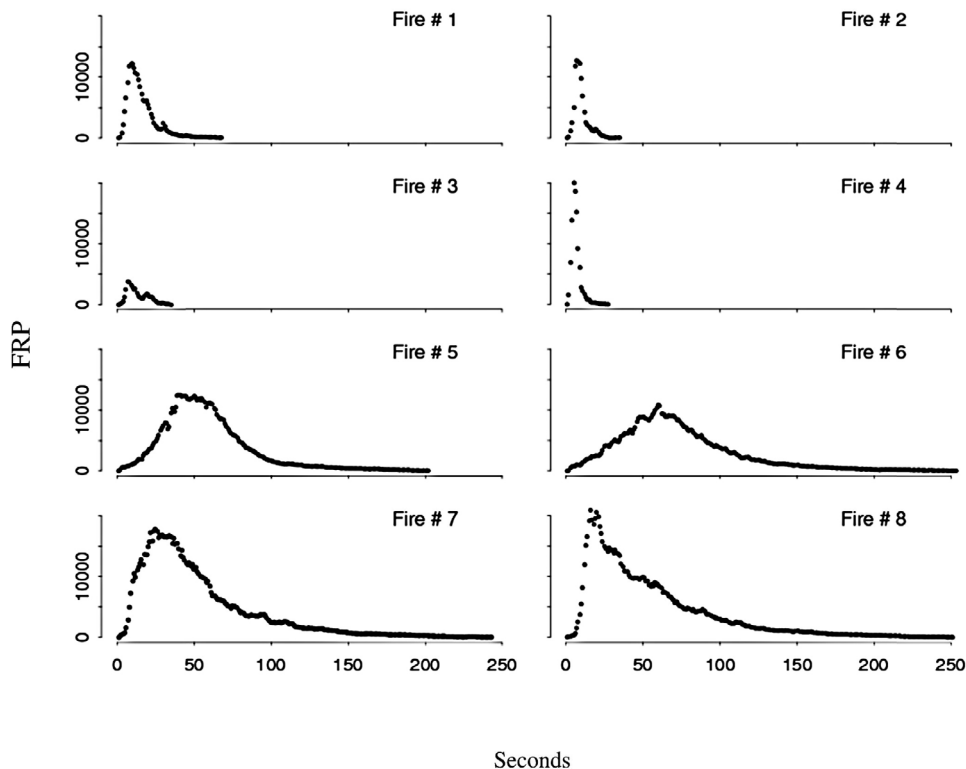


Figure 1. Temporal evolution of FRP (units: W m⁻²) measured at 10 s intervals for eight prescribed fires (Table 1). The start of the fire was defined as the time the FRP increased above the background prefire temperature and the end of the fire as the time when the measured temperature dropped below the prefire temperature.

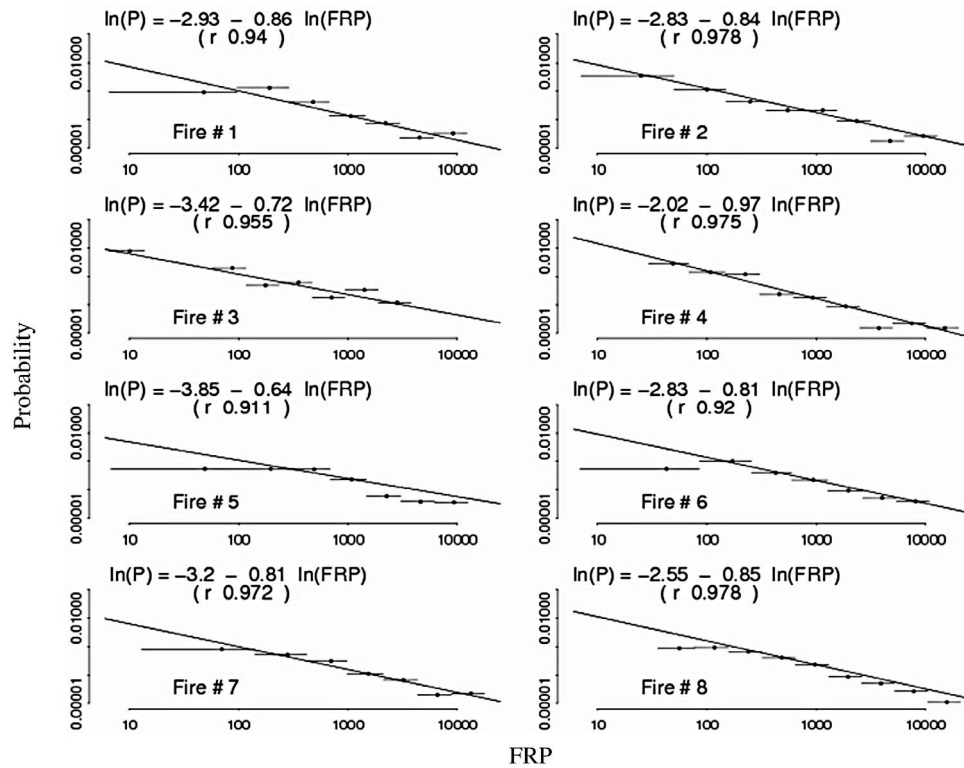


Figure 2. Power law fit to the FRP (units: W m^{-2}) data illustrated in Figure 1. The regression coefficients are shown in each plot. The FRP probability distribution functions, $P(\text{FRP})$, in log-log scales are illustrated with the horizontal bars showing the width of each bin with nonzero $P(\text{FRP})$. For fires 1, 5, 6, and 7 the first bin has a nonzero $P(\text{FRP})$, and so the bin width is illustrated as beginning from the logarithm of the minimum FRP value rather than zero.

goodness of fit r and the regression parameters are computed. Increasing the number of bins, n narrows the bin intervals but does not necessarily increase the number of bins with nonzero counts or increase the r value. The binning scheme with the maximum r is selected as the optimal scheme and the associated m and $\log[c]$ regression parameters selected. The $\text{FRE}_{\text{pwr.law}}$ is estimated as (8) using the m value and specified values of d , FRP_{min} , and FRP_{max} .

2.4. Biomass Burned Estimation From FRE

[15] The FRE computed conventionally as (2) or with the power law method as (8), is used to estimate the total biomass burned (units: g) using an established linear relationship between the FRE (J) and the biomass burned as follows:

$$\text{Biomass Burned} = 0.368 \times 10^3 \text{ FRE}, \quad (13)$$

where 0.368 is a constant derived from experimental data, with an uncertainty of ± 0.015 defining the 95% confidence intervals [Wooster *et al.*, 2005]. Literature estimates of burned biomass (fuel consumed per unit area) are typically reported in terms of kg m^{-2} . Accordingly, in this paper, the FRP data retrieved from satellite- and field-based radiometers are divided by the surface area sensed by the instrument detector to give FRP data in terms of W m^{-2} . In

this way, the FRE derived as (2) or (8) is defined in terms of $J \text{ m}^{-2}$ and the biomass burned in terms of kg m^{-2} .

3. Demonstration of FRE Estimation Methods With Eight U.S. Prescribed Fires

[16] Eight experimental prescribed fires were ignited on 4 m square plots on a prepared bare mineral soil surface at the USDA Forest Service Vinton Furnace experimental forest site, Columbus, Ohio. The fuels were varying mixtures of eastern U.S. hardwood litter and woody types (1 and 10 h fuels) that burned for different lengths of time depending on the fuel loading and composition (Table 1). A dual band (long wave infrared and mid wave infrared) radiometer and downward-looking video camera developed for wildland fire monitoring were mounted approximately 4 m above the center of each plot. The dual-band radiometer (field of view = 60°) was calibrated for radiance against a standard laboratory blackbody source, while the video camera was used to observe the fire extent. Other synchronized video cameras were used to measure flame height and fire front location. Witness targets were placed in the fire to allow measurements to be made of the fire extent relative to the field of view of the radiometer. The brightness temperature of the fire was inferred using a laboratory-derived calibration that related the ratio of the midwave infrared to long-wave infrared radiance to the brightness temperature [Kremens

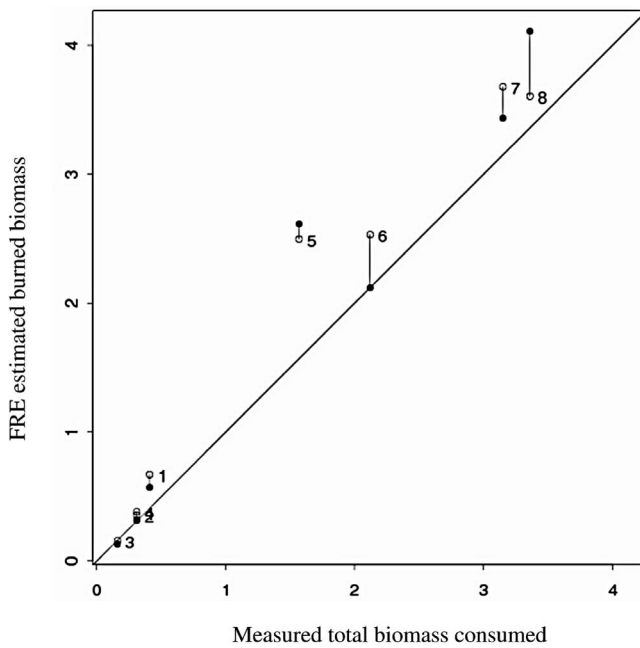


Figure 3. Comparison of burned biomass (units: kg m^{-2}) estimated using FRE computed by (filled circles) $FRE_{\text{pwr.law}}$ and (open circles) $FRE_{\text{num.int}}$ with the measured total biomass consumed (Table 1) for the eight prescribed fires illustrated in Figure 1. The solid line shows the 1:1 line for reference. The FRE values were computed independently for each fire, i.e., the eight $FRE_{\text{pwr.law}}$ values were derived using the power law fit approach as (8), with FRP_{min} , FRP_{max} , fire duration d , and the m regression parameter estimated from the FRP measurements for each fire, and the eight $FRE_{\text{num.int}}$ values were derived by summing the FRP measurements for each fire as (2).

et al., 2010]. With the use of this method, the fire emissivity and fire fractional area (areal fraction of radiometer field of view) product was obtained along with the brightness temperature, from which the emitted radiant power was derived [Riggan *et al.*, 2004; Kremens *et al.*, 2010; Daniels, 2007]. The fire radiant flux was measured at 10 s intervals for the duration of each fire, starting before the fire was lit and lasting until the fire was completely extinguished. The FRP [W m^{-2}] was computed from these estimates using the Stefan-Boltzmann equation [Kaufman *et al.*, 1998]. The prefire and postfire fuel loads were measured using an accurate scale, and their difference was used to derive the total biomass consumed.

[17] Figure 1 shows the FRP (units: W m^{-2}) plotted as a function of time for the eight fires; the FRP rises sharply during the initial stages of the fire, peaks, and then decays slowly. Fire 8 consumed the maximum total fuel (litter and woody, Table 1) and burned with the highest measured FRP ($20,887 \text{ W m}^{-2}$) compared with the other fires. Fire 4 was fueled only by dry litter, burned for the shortest duration (260 s), and burned energetically with a maximum FRP ($20,029 \text{ W m}^{-2}$) comparable to Fire 8. Fire 3 consumed the least total fuel and burned with the lowest maximum FRP (3786 W m^{-2}).

[18] Figure 2 shows the power law fit derived using the method described in the previous section applied to the FRP

measurements for each prescribed fire. Both axes are shown with logarithm scales. Fire 5 has the lowest correlation ($r = 0.91$) between the robust regression predicted and observed FRP probability, and fire 8 has the highest correlation ($r = 0.98$). These results indicate that the FRP probability distribution for the eight fires has a power law behavior. For the eight fires the correlations between the total fuel consumed and the fire duration (d), the maximum FRP, the slope of the power law fit (m), and the product of d and m is 0.932, 0.518, 0.105, and 0.959, respectively. This is expected as the total fuel consumed is directly proportional to the FRE (13), which is a function of the fire duration and the shape of the FRP probability distribution (8).

[19] Figure 3 illustrates the burned biomass estimates derived as (13) from $FRE_{\text{pwr.law}}$ (filled circles) and from $FRE_{\text{num.int}}$ (open circles) plotted against the measured total biomass consumed (Table 1). The $FRE_{\text{num.int}}$ values were estimated independently for each fire by application of (2). The $FRE_{\text{pwr.law}}$ values were estimated independently for each fire as (8) using the FRP_{min} , FRP_{max} , and d values (Table 1) and the estimated power law slope values (m) illustrated in Figure 2. The FRE-derived burned biomass estimates (y axis) are quite similar to the total biomass consumed measurements (x axis). For the low fuel load fires (fires 1–4), the absolute difference between the FRE based and the measured total biomass consumed is less than 0.16 kg m^{-2} . The largest difference is for fire 5, the fire with the lowest power law goodness of fit ($r = 0.91$; Figure 2), with a difference of 1 kg m^{-2} and 0.93 kg m^{-2} for the $FRE_{\text{pwr.law}}$ and $FRE_{\text{num.int}}$ estimates, respectively. Over all eight fires, the mean absolute relative percentage difference, computed as $(100 \times \text{mean} [(FRE \text{ estimated biomass burned} - \text{total biomass consumed})/\text{total biomass consumed}])$ is 19.9% and 25.9% for the $FRE_{\text{pwr.law}}$ - and $FRE_{\text{num.int}}$ -based burned biomass estimates, respectively. Evidently, the new $FRE_{\text{pwr.law}}$ estimation method may provide an alternative to the conventional numerical integration method $FRE_{\text{num.int}}$. The absolute difference between the FRE-based and the measured total biomass consumed is greater for the higher biomass consumption fires; this may be due to insufficient FRP sampling, inaccuracy in the radiometer FRP retrievals, or error in the multiplicative factor (0.368) used in (13) to derive biomass burned from FRE. Simple linear regression of all the data plotted in Figure 3 indicates that a multiplicative factor of 0.313 would provide a better fit of the estimated and measured biomass consumed. However, because we have no way of establishing which factor(s) are causing these differences we, use the 0.368 multiplicative factor prescribed by Wooster *et al.* [2005] for this research.

[20] The sensitivity of the FRE estimation methods under progressively sparser FRP sampling was investigated by randomly selecting without replacement 90%, 60%, 30%, and 15% of the FRP measurements for each fire. The FRP subsample data for each fire were ordered chronologically and used to independently compute $FRE_{\text{num.int}}$ as (2), and to compute $FRE_{\text{pwr.law}}$ as (8) using FRP_{min} , FRP_{max} , d , and m values derived from the FRP subsample data. This simulation was repeated 1000 times and each time the biomass burned was computed as (13) from the $FRE_{\text{num.int}}$ and $FRE_{\text{pwr.law}}$ estimates. Figure 4 shows the results derived from the 1000 sparsely sampled FRP subsets; each colored dot shows the results of one simulation, and each of the eight fires

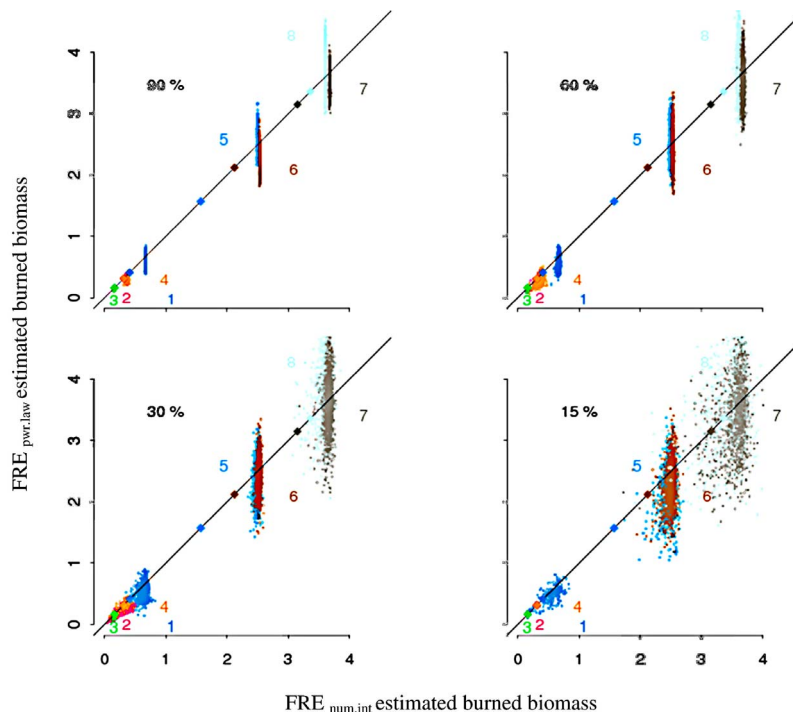


Figure 4. Comparison of burned biomass (units: kg m^{-2}) estimated from $FRE_{\text{pwr.law}}$ and $FRE_{\text{num.int}}$ for the 8 prescribed fires under simulated sparse FRP sampling conditions (90%, 60%, 30%, and 15% FRP subsampling). The undersampled FRP data for each fire were used to independently compute $FRE_{\text{num.int}}$ and $FRE_{\text{pwr.law}}$ for 1000 simulations (circular colored dots) for fires 1–8 (dark blue, red, green, light blue, orange, brown, gray, and cyan, respectively). The colored diamonds show the measured total biomass consumed (same values plotted in the Figure 3 x axis).

is represented by a unique color. The scatter in the colored dots is the least for the 90% subsample and the greatest for the 15% subsample, reflecting the sensitivity of FRE computation by both methods to decreasing the number of FRP measurements. The spread of the colored dots illustrated in Figure 4 implies that, while both methods of FRE estimation have significant uncertainty with smaller subsample sizes, $FRE_{\text{num.int}}$ is less sensitive than $FRE_{\text{pwr.law}}$. The colored diamonds in Figure 4 show the total biomass consumed measurements for each fire (Table 1) and are offset from the colored dots in the same way as the results computed without FRP subsampling illustrated in Figure 3.

[21] Figure 5 shows the results of a new simulation. The $FRE_{\text{pwr.law}}$ biomass burned values were computed with the fire duration derived independently as Figure 4 from the FRP subsample data, but with the fixed FRP power law parameters (m , FRP_{min} , and FRP_{max}) derived from all of each fire's FRP data. Thus, the $FRE_{\text{pwr.law}}$ biomass burned values will only vary with the fire duration estimates. The $FRE_{\text{num.int}}$ biomass burned values were derived as for Figure 4. In Figure 5 the $FRE_{\text{pwr.law}}$ and $FRE_{\text{num.int}}$ biomass burned estimates are similar for the 90% and 60% subsampling. However, the scatter in the $FRE_{\text{pwr.law}}$ biomass burned estimates is smaller than the scatter in the $FRE_{\text{num.int}}$ estimates for the sparser 30% and 15% subsampling. This is in contrast with the results plotted in Figure 4, and implies that if the power law parameters (m , FRP_{min} , FRP_{max}) can be characterized reliably a priori, then $FRE_{\text{pwr.law}}$ is less sensitive to FRP undersampling than the conventional $FRE_{\text{num.int}}$

numerical integration method. Figure 6 confirms this, showing summary statistics of the relative percentage differences between the burned biomass estimated using all of the FRP data (illustrated in Figure 3) and the burned biomass estimated from the undersampled FRP data (illustrated in Figure 5). For progressively more severe FRP undersampling, the mean and standard deviation of the $FRE_{\text{pwr.law}}$ biomass burned differences generally become smaller than the corresponding $FRE_{\text{num.int}}$ differences. The mean differences do not change much for fires 5–8, for either FRE estimation method, perhaps because, for these fires, the FRP data captured the FRP temporal variability (>200 observations every 10 s) more completely than for fires 1–4 (<70 observations every 10 s) that burned for much shorter durations (Table 1).

4. Development of FRE Estimation Methods With MODIS Data

4.1. MODIS Active-fire and FRP Data

[22] The MODIS sensor is onboard the polar-orbiting Terra (10.30AM Equatorial overpass time) and Aqua (1.30PM Equatorial overpass time) satellites providing up to four day and nighttime active-fire detections and corresponding FRP estimates for a pixel at the Equator [Giglio *et al.*, 2003]. The MODIS is a whiskbroom sensor, such that the ground area sensed by each detector increases with scan angle; for example, a 1 km detector senses an area of approximately 1.0 by 1.0 km at nadir, but, at the edge of the scan, senses an area of approximately 2.01 by 4.83 km in the

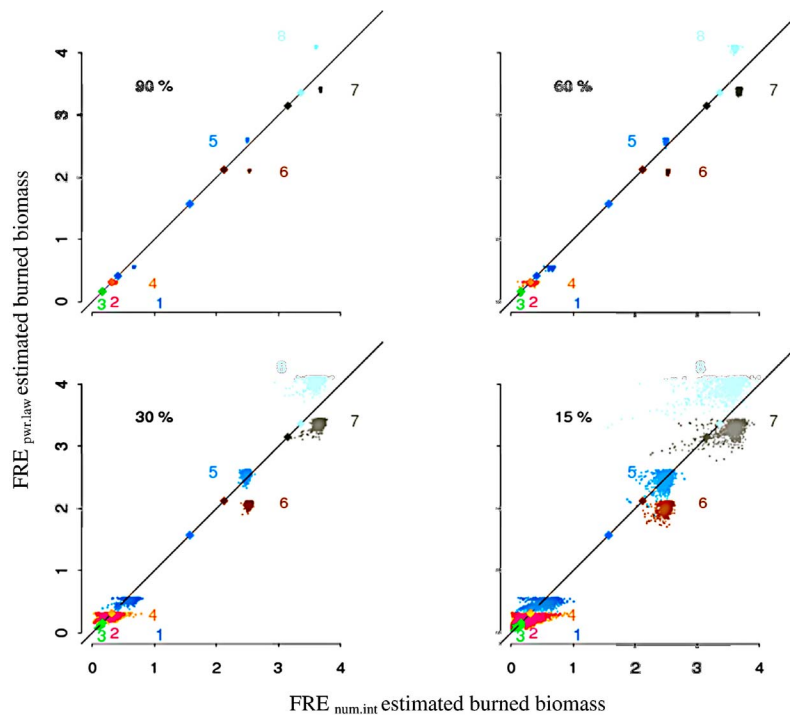


Figure 5. Comparison of burned biomass (units: kg m^{-2}) estimated from $FRE_{\text{pwr.law}}$ and $FRE_{\text{num.int}}$ for the eight prescribed fires under simulated sparse FRP sampling conditions (90%, 60%, 30%, and 15% FRP subsampling). The undersampled FRP data for each fire were used to independently compute $FRE_{\text{num.int}}$ and $FRE_{\text{pwr.law}}$ for 1000 simulations (circular colored dots) for fires 1–8 (dark blue, red, green, light blue, orange, brown, gray, and cyan, respectively). The $FRE_{\text{num.int}}$ biomass results are the same as in Figure 4; the $FRE_{\text{pwr.law}}$ -derived biomass burned values were computed keeping m , FRP_{min} , and FRP_{max} fixed and defined from all the FRP measurements of the fire and with only the fire duration defined from the undersampled FRP. The colored diamonds show the measured total biomass consumed (same values plotted in the Figure 3 x axis).

along-track and along-scan directions, respectively [Wolfe *et al.*, 1998]. The Collection 5 MODIS Terra and Aqua Level 2 active-fire products used in this study are defined with this geometry, and define for each 1 km (at nadir) observation whether an active fire was detected, the confidence level of the detection, and the FRP in MW. The MODIS FRP is estimated using an empirical relationship between the FRP and brightness temperature retrieved in the midinfrared and is not expected to saturate over hot and/or large vegetation fires [Kaufman *et al.*, 1998; Ichoku *et al.*, 2008]. If no MODIS active fire was detected then the surface status (land, water, cloud, or unknown) is defined.

[23] For most of the analyses in this study, the MODIS Level 2 FRP data were converted to (MW km^{-2}) by dividing the FRP (units: MW) by the sensed ground area (units: km^2) [Ichoku and Kaufman, 2005]. In addition, for certain analyses, the Level 2 FRP data were reprojected to the gridded 1 km Level 3 MODIS sinusoidal equal area projection [Wolfe *et al.*, 1998]. In the reprojection process, the FRP (MW) of each Level 2 active-fire observation was divided by the number of Level 3 pixels it encompassed such that the total FRP in each Level 3 gridded data set was equal to the total FRP in the original Level 2 data [Boschetti and Roy, 2009]. The Level 3 FRP were defined in MW km^{-2} .

4.2. Australian and Brazilian Study Areas

[24] Two study areas with contrasting prefire fuel loads and fire behavior were selected, one over Australian tropical savanna and the other over Brazilian deforestation. Over the Australian study area, 3660 MODIS Level 2 active fires were detected from 27 September to 7 November 2002 (1884 Aqua and 1776 Terra), with MODIS FRP values for individual fire pixels ranging from 5.754 to 1937.893 MW. Over the Brazilian study area, 409 MODIS Level 2 active fires were detected from 6 January to 20 December 2003, with MODIS FRP values ranging from 8.074 to 7230.168 MW. Figure 7 plots the spatially explicit Level 2 detections over each study area.

[25] The Australian study area is defined by a MODIS mapped burned area that burned approximately $14,675 \text{ km}^2$ and is located between $131^\circ\text{--}133^\circ\text{E}$, $16^\circ\text{--}18^\circ\text{S}$ at the border of the Sturt Plateau and the Ord-Victoria Plains in the Northern Territories [Boschetti and Roy, 2009]. The vegetation is predominantly spinifex grasses with sparse (<10% cover) trees with an average fuel load of 0.78 kg m^{-2} (Sturt Plateau) and 0.81 kg m^{-2} (Ord Victoria Plains) [Russell-Smith *et al.*, 2003]. In this region the burning efficiency, defined as the product of the combustion completeness and the proportion of the satellite pixel that effectively burned is reported to be 0.72 [Russell-Smith *et al.*, 2003]. The product

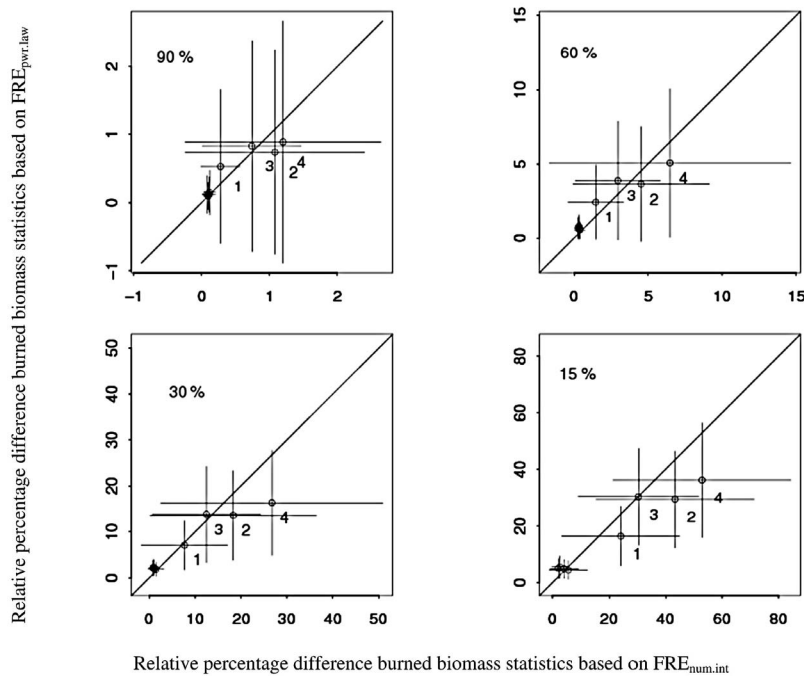


Figure 6. Summary statistics of the relative percentage difference between the burned biomass values estimated from the undersampled FRP data (illustrated in Figure 5) and the burned biomass estimated using all of the FRP data without undersampling (illustrated in Figure 3). The percentage difference for each simulation (colored dot in Figure 5) is estimated as $|\text{Burned biomass}_{\text{under sampled}} - \text{burned biomass}_{\text{without undersampling}}| / \text{burned biomass}_{\text{without undersampling}}$. The mean of the percentage differences (circles) and the standard deviation around the mean (horizontal and vertical lines) is shown for the $FRE_{\text{pwr.law}}$ (y axis) and $FRE_{\text{num.int}}$ (x axis) methods for fires 1–8. Fires 1–4 are labeled, fires 5–8 are clustered near the plot origin and are not labeled.

of the average of the two fuel load estimates and burning efficiency provides a comparison biomass burned estimate of 0.57 kg m^{-2} [Boschetti and Roy, 2009].

[26] The Brazilian study area is a $0.12^\circ \times 0.12^\circ$ region centered at 13.1°S , 56.57°W close to the “arc of deforestation” in the state of Mato Grosso with a high density of

MODIS active-fire detections. Visual inspection of multi-date Landsat acquisitions indicated large areas of deforestation and subsequent burning between January and December 2003. There is no definitive fuel load or consumption information available for the study area. A 1 km spatially explicit biomass classification data set with a reported 70%

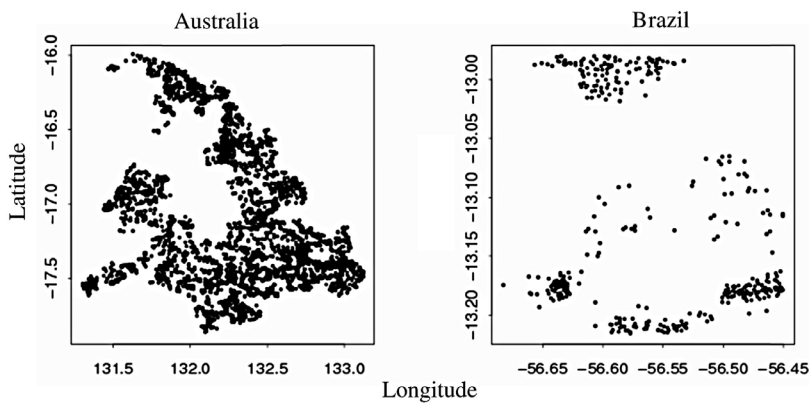


Figure 7. Locations of MODIS Aqua and Terra day and nighttime active-fire detections over the (left) Australian and (right) Brazilian study areas. A total of 3,660 Level 2 active fires were detected from 27 September to 7 November 2002 over the Australian study area (1884 Aqua and 1776 Terra), with FRP ranging from 5.754 MW to 1937.893 MW. A total of 409 Level 2 active fires were detected over the Brazilian study area (220 Aqua and 189 Terra) from 6 January to 20 December 2003, with FRP ranging from 8.074 MW to 7230.168 MW.

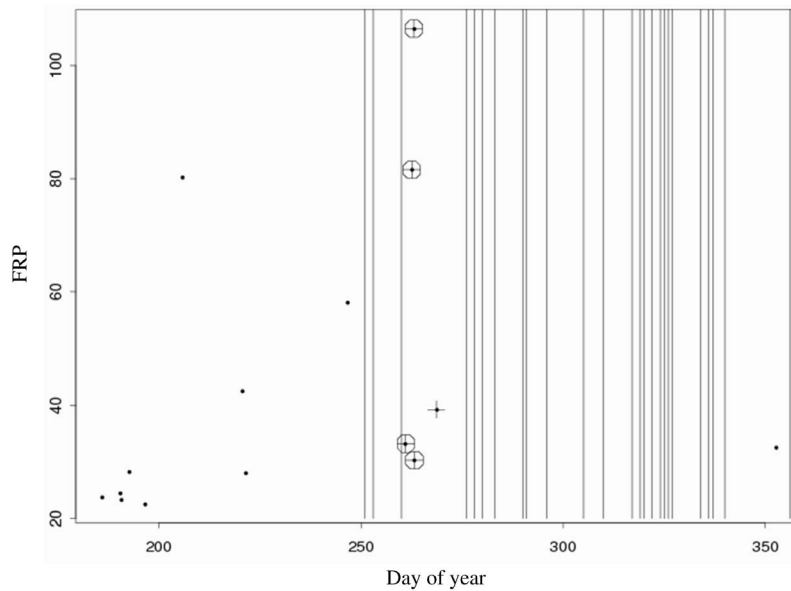


Figure 8. The Level 2 FRP (units: MW) of all the MODIS Terra and Aqua day and nighttime detections within the same 1 km location (13.17083°S , 56.63563°W) in the Brazilian study area plotted against day of year in 2003 (black dots). The vertical lines show days when there were either no MODIS observations of the surface or when all the MODIS observations were cloudy. The absence of vertical lines indicates at least one nonfire MODIS observation for a given day. The circles and cross symbols show the commission error reduction algorithm results generated using a temporal threshold of 4 and 10 days, respectively.

accuracy [Saatchi *et al.*, 2007] was analyzed and provides a mean study area above a ground biomass of 10.77 kg m^{-2} . In the Brazilian state of Mato Grosso, deforestation fires burn with a combustion completeness ranging from 0.2 to 0.6 with a typical value of 0.5 [Carvalho *et al.*, 2001; van der Werf *et al.*, 2008; Soares Neto *et al.*, 2009]. The product of the typical combustion completeness and the mean above-ground biomass provides a comparison biomass burned estimate of 5.38 kg m^{-2} , about ten times greater than for the Australian study area. Similarly, research undertaken at a Mato Grosso site approximately 500 km away from the study area measured burned biomass from 1.5 to 4.45 kg m^{-2} with a standard error of approximately 50% [Balch *et al.*, 2008].

4.3. Brazilian MODIS Active-Fire Commission Error Reduction

[27] The Collection 5 MODIS active-fire product has an estimated 3% commission error over the entire Legal Amazon with more than 35% detected over areas with a mix of high and low percentage tree cover [Schroeder *et al.*, 2008]. A worst case scenario is illustrated in Figure 8, which shows the FRP of 15 active fires detected in the study area at the same 1 km location occurring over an implausibly long 167 day period. Typically, the maximum duration of deforestation fires is 15 days [Morton *et al.*, 2008]. In an attempt to reduce the impact of this commission error, the Aqua and Terra FRP values were temporally filtered and only collocated FRP values occurring within a temporal duration of n days (4, 6, 8, or 10 days) from each other, and that included the active-fire detection with the maximum FRP over the year, were considered. This filtering was implemented during the Level 2 to Level 3 reprojection and gridding process (section 4.1), so that, for each filtered

Level 3 FRP value, its filtered parent Level 2 FRP value was retained. The circles and crosses in Figure 8 show the active-fire detection Level 2 FRP values retained by the use of a temporal duration threshold of 4 and 10 days, respectively. Evidently, a longer duration threshold allows more active detections to be retained. We have no reliable way of validating this method, and so analyses of the estimated FRE and biomass burned with respect to different temporal duration thresholds is described in section 5.2.2.

4.4. MODIS FRP_{\min} , FRP_{\max} and Fire Duration Estimation

[28] The, FRP_{\min} , FRP_{\max} , and fire duration are needed to determine $FRE_{\text{pwr.law}}$ (8). These values may either be prescribed, for example, from available field studies or observations, or can be estimated from the MODIS Terra and Aqua data. The FRP_{\min} and FRP_{\max} were set as the minimum and maximum observed Level 2 MODIS Terra and Aqua FRP for each study area. Sensitivity of $FRE_{\text{pwr.law}}$ to the choice of FRP_{\min} and FRP_{\max} for each study area is presented in section 5.3.

[29] The fire duration was estimated from the MODIS active-fire detections by comparison of the dates and time of the MODIS Terra and Aqua detections (up to four per 24 h) [Loboda and Csizsar, 2007; Boschetti and Roy, 2009]. Spatially explicit fire durations (units: s) were computed for each Level 3 pixel as the temporal difference between the times of the MODIS observations with no active-fire detection that preceded and followed the first and last active-fire detection(s), respectively. Pixels identified as clouds in the MOD14 product were assumed to have not burned to avoid overestimation of the fire duration [Boschetti and Roy, 2009]. We recognize that the Level 2 to

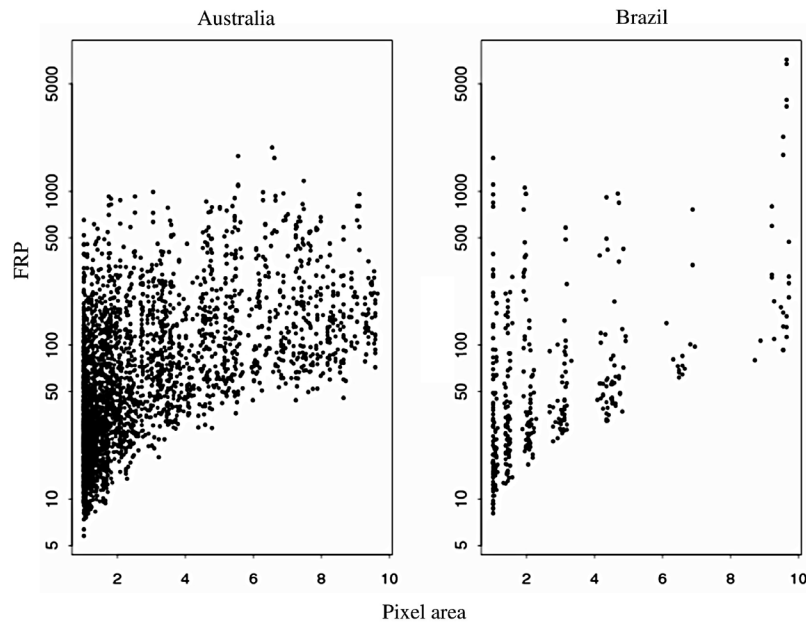


Figure 9. MODIS Level 2 FRP (units: MW) plotted against the sensed surface area (units: km²). The FRP values are plotted in natural logarithmic scales for visual clarity. The plot includes all the detections shown in Figure 6 for each study area. Note that MODIS observations have a larger sensed surface area at a greater scan angle further from the nadir.

Level 3 reprojection process will “artificially” increase the number of times a Level 3 pixel will have a fire detected within it. This may increase the number of shorter-duration fires or inflate the duration. Despite these limitations, this method has been shown to be useful [Loboda and Csiszar, 2007; Boschetti and Roy, 2009].

4.5. Adaptation of the FRE Power Law Fit Method to Correct for MODIS FRP Omission Errors

[30] The FRP is defined for each MODIS active-fire detection. However, the MODIS active-fire product can only detect fires that are sufficiently hot and/or large depending on the areal proportions and temperatures of the nonburning and the smoldering and flaming fire components [Kaufman *et al.*, 1998; Giglio and Justice, 2003]. This sensitivity is known to cause a systematic detection omission of cool and/or small fires [Giglio *et al.*, 2003], particularly those with low FRP [Schroeder *et al.*, 2008; Freeborn *et al.*, 2009]. Underestimation of FRP may also occur depending on the suppixel location of the active fire with respect to the central pixel location [Calle *et al.*, 2009; Schroeder *et al.*, 2010]. In addition, at increasingly higher MODIS scan angles, where the sensed ground area is larger, only larger and/or hotter fires tend to be detected [Giglio *et al.*, 1999; Mottram *et al.*, 2005; Freeborn *et al.*, 2011]. The resulting underestimation of the number of active fires detected with low FRP at high scan angles is evident in Figure 9, which shows the MODIS Level 2 FRP values and the corresponding sensed ground areas for the Australian and Brazilian study areas. Roberts *et al.* [2005] and Roberts and Wooster [2008] observed similar FRP omission errors in African geostationary (SEVIRI) FRP data. Roberts *et al.* [2005] suggested, and illustrated qualitatively, that fitting a reciprocal exponential distribution function to the SEVIRI FRP histogram

may provide a way to extrapolate the FRP distribution to lower values to correct for satellite FRP omission effects.

[31] We adopted an approach similar to that suggested by Roberts *et al.* [2005] to correct for MODIS low FRP omission errors. The FRP power law fit methodology (section 2.3) was applied to the Level 2 FRP data (MW km⁻²) after ignoring all the lower value FRP bins with P (FRP) smaller than the bin with $\max[P(FRP)]$. In this way, we extrapolate the regression fit to the lowest observed FRP to compensate for any low FRP omission effects.

4.6. MODIS FRE and Biomass Burned Estimation

[32] Conventional numerical integration and power law based FRE estimates and corresponding biomass burned estimates were derived for the study areas. The Brazilian estimates were computed with FRP data sets filtered using 4, 6, 8, and 10 day temporal duration thresholds to examine the sensitivity of the estimates to the commission error reduction approach (section 4.3). Both spatially explicit (different estimate for each active fire detection pixel) and spatially nonexplicit (a single estimate for the study area) estimates were made in the same way as reported by Boschetti and Roy [2009] and are described in detail below.

[33] Spatially non-explicit FRE values were computed assuming that the multiple FRP values retrieved over the study area were from a single fire event that burned progressively between the first and last active-fire detection; i.e., fires propagating from a single or multiple simultaneous ignitions scattered throughout the study area [Boschetti and Roy, 2009]. In this way, a single $FRE_{num.int}$ value was computed by numerical integration of all the Level 2 FRP values (MW km⁻²) over the study area and period. The FRP values were ordered chronologically and summed as (2); if more than one active fire was detected on the same day and

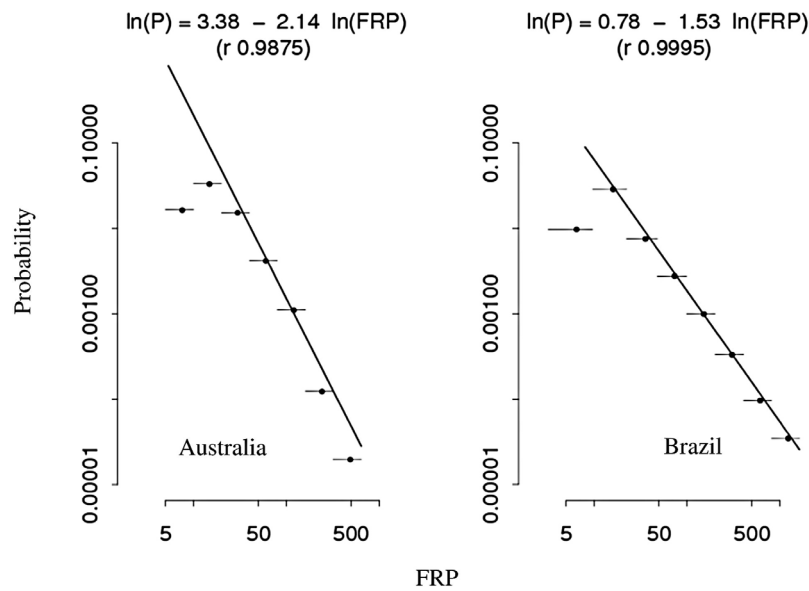


Figure 10. Power law fit of the (left) Australian and (right) Brazilian study area Aqua and Terra MODIS Level 2 FRP (units: MW km^{-2}) data. The slope (scaling parameter m) of the power law fit for the Australian FRP data is 2.1446 and for the Brazilian FRP data is 1.5345. The Brazilian study area power law fits are shown for 177 FRP Level 2 detections (92 Aqua and 85 Terra) selected from the 409 original values using a 4 day commission error reduction threshold as an example.

at the same time, then they were summed and treated as a single FRP value. A single $FRE_{\text{pwr.law}}$ estimate was computed as (8) using power law characteristics (m , FRP_{min} , and FRP_{max}) derived from all the Level 2 FRP values and with a single fire duration derived by the difference in time between the last and the first FRP retrieval. All the FRP data were used to derive m , FRP_{min} , and FRP_{max} , because this provides $FRE_{\text{pwr.law}}$ estimates that are less sensitive to sparse FRP sampling for the prescribed fire data (Figures 5 and 6) and assumes that the FRP distribution characteristics, i.e., the fuels, conditions, and fire behavior, are the same for all the fires in the study area.

[34] Spatially explicit FRE values were computed for each Level 3 pixel location where there were FRP values retrieved over the study period. The spatially explicit $FRE_{\text{num.int}}$ was computed at each Level 3 pixel by summation as (2) considering the Level 3 FRP value(s) (MW km^{-2}) and their time of detection. The spatially explicit $FRE_{\text{pwr.law}}$ was computed as (8) using the spatially explicit fire duration estimates (section 4.4) and using power law characteristics (m , FRP_{min} , and FRP_{max}) derived from all the Level 2 FRP data (MW km^{-2}) over the study area.

5. MODIS Results

5.1. MODIS FRP Power Law Fitting

[35] Figure 10 shows the power law fits of the Australian (Figure 10, left) and Brazilian (Figure 10, right) MODIS Level 2 FRP data. The points show the probability distribution of the FRP values, and the horizontal line segments show the probability distribution bin widths. The Brazilian FRP data set was filtered with a 4 day temporal duration threshold. The power law fits (lines) are shown computed for both Aqua and Terra FRP data. The power law fits were adapted for the MODIS omission errors by ignoring all the

lower value FRP bins with $P(\text{FRP})$ smaller than the bin with $\max[P(\text{FRP})]$ and extrapolating the fits to the lowest observed FRP values. As expected, the FRP probability distributions deviate from a linear behavior for the low-value FRP bins.

[36] For both study areas, a high correlation is found between the predicted and observed FRP probability values, 0.9874 and 0.9983 for Australia and Brazil, respectively, indicating that the MODIS FRP data exhibit a power law behavior. The scaling parameters (m), i.e., the slopes of the linear power law fits illustrated in Figure 10, are 2.14 and 1.53 for the Australian and Brazilian data, respectively. This implies that the Australian fires have a relatively greater proportion of lower value FRP values than higher values in comparison with the Brazilian study area fires. This is expected as the vegetation at the Australian study area is predominantly spinifex grass which should burn less energetically than the Brazilian deforestation fires which have a higher fuel load and perhaps larger actively flaming fire fronts.

5.2. MODIS FRE and Burned Biomass Estimation

5.2.1. Australian Study Area Results

[37] The Australian nonspatially explicit $FRE_{\text{num.int}}$ and $FRE_{\text{pwr.law}}$ estimated values were 1.2594 and 1.2565×10^6 MJ km^{-2} , respectively, providing burned biomass estimates of 0.4634 and 0.4624 kg m^{-2} , respectively, that are comparable (about 81%) to the study area 0.57 kg m^{-2} comparison burned biomass estimate described in section 4.2. The similarity of these results indicates that the MODIS FRP sampling was perhaps sufficient to capture the fire FRP variability when considered in a non-spatially explicit manner.

[38] Australian spatially explicit $FRE_{\text{num.int}}$ and $FRE_{\text{pwr.law}}$ values were derived at each of 6539 Level 3 pixels where one or more MODIS Terra or Aqua FRP values were

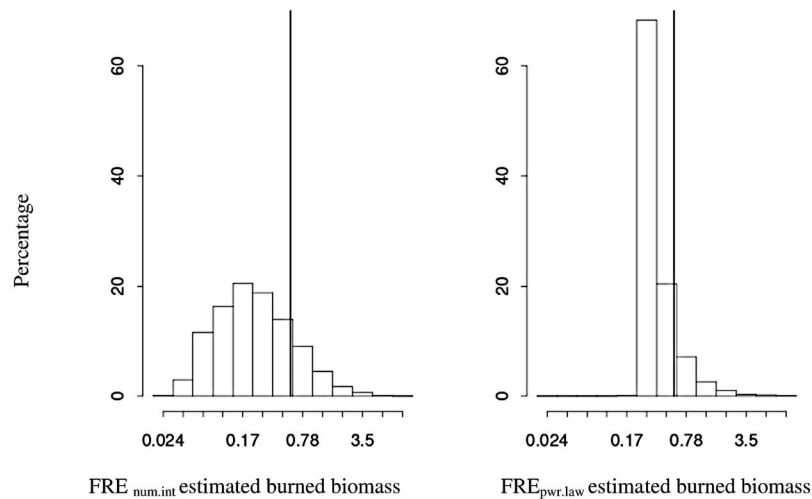


Figure 11. Histograms of the Australian study area MODIS Terra and Aqua spatially explicit FRE-derived biomass burned estimates (units: kg m^{-2}) derived from (left) $FRE_{\text{num.int}}$ and (right) $FRE_{\text{pwr.law}}$. The histograms are shown log-transformed for illustrative clarity. The results were derived at the same 6539 Level 3 1 km pixel locations. The vertical dashed lines show the study area 0.57 kg m^{-2} comparison burned biomass estimate. A total of 6539 Level 3 FRP data values (MW km^{-2}) were used to derive $FRE_{\text{num.int}}$ and the fire durations required to estimate $FRE_{\text{pwr.law}}$. A total of 3660 Level 2 FRP (MW km^{-2}) values were used to infer the power law scaling parameters m , FRP_{min} , and FRP_{max} .

detected. Figure 11 shows histograms of the Australian spatially explicit biomass burned results. The $FRE_{\text{num.int}}$ -based biomass estimates (Figure 11, left) are more widely scattered than the $FRE_{\text{pwr.law}}$ -based estimates (Figure 11, right). The medians of the spatially explicit $FRE_{\text{num.int}}$ - and $FRE_{\text{pwr.law}}$ -based biomass burned estimates are 0.2149 and 0.3393 kg m^{-2} , respectively, corresponding to 38% ($FRE_{\text{num.int}}$ -based) and 60% ($FRE_{\text{pwr.law}}$ -based) of the study area 0.57 kg m^{-2} comparison biomass burned value. The power law based median is closer to the comparison estimate. This pattern is similar to that found for the prescribed fire FRP subsampling results illustrated in Figure 5 and is most likely because the spatially explicit $FRE_{\text{pwr.law}}$ estimates were computed using the power law characteristics (m , FRP_{min} , and FRP_{max}) derived from all the Australian FRP data. For both the conventional and power law methods, there were some unrealistically high biomass estimates, 10% of the $FRE_{\text{num.int}}$ and 6% of the $FRE_{\text{pwr.law}}$ pixels had burned biomass values greater than 0.81 kg m^{-2} (the highest available fuel load reported in the literature). These high values may be due to isolated energetic burning of eucalyptus trees in the study

area and/or due to insufficient FRP sampling at those pixel locations [Boschetti and Roy, 2009].

5.2.2. Brazilian Study Area Results

[39] The Brazilian nonspatially explicit $FRE_{\text{num.int}}$ and $FRE_{\text{pwr.law}}$ values and biomass burned estimates computed using FRP data sets filtered with 4, 6, 8, and 10 day temporal duration thresholds are summarized in Table 2. In all cases, for both the conventional and power law methods and for all duration thresholds, the FRE-derived burned biomass estimates are significantly greater by factors of about 3 ($FRE_{\text{num.int}}$) and 4.5 ($FRE_{\text{pwr.law}}$) than the study area comparison 5.38 kg m^{-2} estimate. These poor Brazilian results are likely because the fires were not from the same progressively burning fire event, which is an implicit assumption of the nonspatially explicit FRE computation [Boschetti and Roy, 2009]. The Brazilian fires clearly occurred in different localities (Figure 7, right) and over a 348 day period.

[40] Figure 12 shows histograms of the spatially explicit Brazilian biomass burned results generated from the 4 day temporal-threshold-filtered FRP data. The histograms have very similar distributions for the 6, 8, and 10 day thresholded

Table 2. Nonspatially Explicit FRE and Biomass Burned Estimates for the Brazilian Study Area Derived Using the Numerical Integration ($FRE_{\text{num.int}}$) and Power Law ($FRE_{\text{pwr.law}}$) Estimation Methods for Different Temporal Duration Thresholds^a

Temporal Duration Threshold (day)	Number of Duration Filtered FRP Values Used	$FRE_{\text{num.int}}$ Estimate (10^6 MJ km^{-2})	$FRE_{\text{pwr.law}}$ Estimate (10^6 MJ km^{-2})	$FRE_{\text{num.int}}$ Biomass Burned Estimate (kg m^{-2})	$FRE_{\text{pwr.law}}$ Biomass Burned Estimate (kg m^{-2})
4	177	64.3393	72.2679	23.6769	26.5946
6	186	44.2131	65.2294	16.2704	24.0044
8	192	44.5406	80.3759	16.3909	29.5783
10	194	44.3262	80.3759	16.312	29.5783

^aThe comparison burned biomass estimate for the study area is 5.38 kg m^{-2} . Level 3 FRP data (MW km^{-2}) were used to derive $FRE_{\text{num.int}}$ and the fire durations required to estimate $FRE_{\text{pwr.law}}$. The power law scaling parameters m , FRP_{min} , FRP_{max} were derived from Level 2 FRP (MW km^{-2}) values.

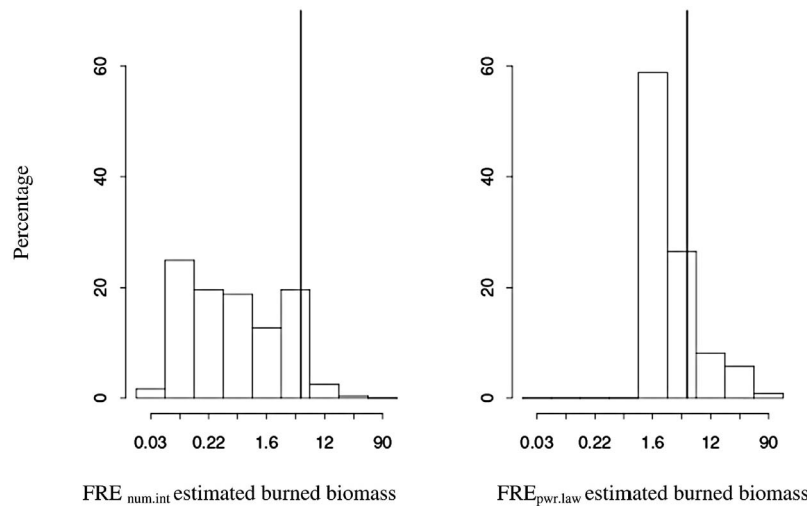


Figure 12. Histograms of the Brazilian study area MODIS Terra and Aqua spatially explicit FRE-derived biomass burned estimates (units: kg m^{-2}) derived from (left) $FRE_{\text{num.int}}$ and (right) $FRE_{\text{pwr.law}}$. The histograms are shown log-transformed for illustrative clarity. The results were derived for the same 245 Level 3 pixel locations. The FRP data set was filtered using a temporal duration threshold of 4 days. The vertical dashed lines show the study area 5.38 kg m^{-2} comparison burned biomass estimate. A total of 245 Level 3 FRP data values (MW km^{-2}) were used to derive $FRE_{\text{num.int}}$ and the fire durations required to estimate $FRE_{\text{pwr.law}}$. A total of 177 Level 2 FRP (MW km^{-2}) values were used to infer the power law scaling parameters m , FRP_{min} , and FRP_{max} .

data. The FRP_{min} and FRP_{max} values did not change for the different temporal duration thresholds, even though a large proportion of the 409 MODIS Level 2 active fires were removed by the filtering process (there were 177 and 194 filtered Level 2 FRP data for the 4 day and 10 day thresholds, respectively). Similarly, the power law scaling parameter values (m) did not change significantly, from 1.535 (4 day threshold) to 1.583 (10 day threshold). For all duration thresholds, there were 245 Level 3 pixels with one or more MODIS Terra or Aqua FRP values and at each of these pixels a single FRE and biomass burned estimate was computed. The $FRE_{\text{num.int}}$ biomass estimates (Figure 12, left) are more widely scattered than the $FRE_{\text{pwr.law}}$ biomass estimates (Figure 12, right) similar to that observed for the Australian spatially explicit results (Figure 11) and for the prescribed fire FRP results illustrated in Figure 5. This is again most likely, because the spatially explicit $FRE_{\text{pwr.law}}$ estimates were computed using power law characteristics (m , FRP_{min} , and FRP_{max}) derived from all the filtered FRP data.

[41] Table 3 summarizes the minimum, median, and maximum of the spatially explicit biomass burned estimates for the different temporal thresholds. For both FRE estimation methods, the maximum biomass burned values are unrealistically high, which may be due to insufficient FRP sampling and isolated burning of high biomass at those pixel locations, about 2% of the $FRE_{\text{num.int}}$ and 4% of the $FRE_{\text{pwr.law}}$ pixels had biomass burned values greater than 10.77 kg m^{-2} (the estimated study area above ground biomass). The minimum and the median of the Brazilian spatially explicit biomass burned $FRE_{\text{pwr.law}}$ estimates are, for all temporal duration thresholds, closer (underestimated by a factor between 3 and 4) to the study area comparison estimate than the $FRE_{\text{num.int}}$ estimates (underestimated by a factor

between 13 and 100). Interestingly, the median $FRE_{\text{pwr.law}}$ biomass burned estimates are progressively more similar to the comparison estimate with decreasing duration threshold values, indicating again that the power law method is relatively insensitive to sparse FRP sampling. In contrast, the median $FRE_{\text{num.int}}$ biomass burned estimates are progressively less similar to the study area comparison estimate with decreasing temporal duration threshold values, most likely because of the sensitivity of the $FRE_{\text{num.int}}$ method to decreased FRP sampling. We note, however, that the range of the median biomass burned estimates over the different temporal duration thresholds is relatively small: 0.3791 to 0.4173 kg m^{-2} for the $FRE_{\text{num.int}}$ -based estimates, corresponding to 7% to 8% of the study area 5.38 kg m^{-2} comparison biomass burned value, and 1.5535 to 1.7223 kg m^{-2} for the $FRE_{\text{pwr.law}}$ -based estimates, corresponding to 29% to 32% of the study area comparison value. Similar to the Australian results, the Brazilian power law based median biomass burned estimates are closer to the comparison estimate than the conventional temporal integration based estimates.

5.3. MODIS $FRE_{\text{pwr.law}}$ Estimation Sensitivity Analysis With Respect to FRP_{min} and FRP_{max}

[42] Reliable $FRE_{\text{pwr.law}}$ estimation depends on suitable selection of FRP_{min} , FRP_{max} , and fire duration values. Because the $FRE_{\text{pwr.law}}$ is linearly dependent on the fire duration (8), we do not investigate the sensitivity of the study area $FRE_{\text{pwr.law}}$ biomass burned estimates to the fire duration. Instead, the sensitivity to FRP_{min} and FRP_{max} is examined. These values were estimated from the study area MODIS Terra and Aqua FRP and active-fire detection date and timing data. The FRP_{min} (Australia, 5.254 MW km^{-2} ; Brazil, 7.390 MW km^{-2}) and FRP_{max} (Australia, 641.599

Table 3. Summary Statistics of the Brazilian Study Area Spatially Explicit Biomass Burned Estimates Derived Using the Numerical Integration ($FRE_{num.int}$) and Power Law ($FRE_{pwr.law}$) Estimation Methods for Different Temporal Duration Thresholds^a

Temporal Duration Threshold (days)	$FRE_{num.int}$ Biomass Burned Estimate (kg m^{-2})			$FRE_{pwr.law}$ Biomass Burned Estimate (kg m^{-2})		
	Minimum	Median	Maximum	Minimum	Median	Maximum
4	0.0415	0.3791	32.1199	1.5230	1.7223	28.5984
6	0.0415	0.3840	32.1199	1.4511	1.6409	98.1063
8	0.0415	0.3840	32.1199	1.3737	1.5535	92.8779
10	0.0415	0.4173	32.1199	1.3737	1.5535	92.8779

^aThe summary statistics were computed over 245 Level 3 pixel locations where there were one or more MODIS Terra or Aqua FRP values. The comparison burned biomass estimate for the study area is 5.38 kg m^{-2} . Level 3 FRP data (MW km^{-2}) were used to derive $FRE_{num.int}$ and the fire durations required to estimate $FRE_{pwr.law}$. The power law scaling parameters m , FRP_{min} , FRP_{max} were derived from Level 2 FRP (MW km^{-2}) values.

MW km^{-2} ; Brazil, $1633.533 \text{ MW km}^{-2}$) values were varied systematically by $\sim 2\%$ steps over $\pm 100\%$ ranges, ignoring zero FRP_{min} and FRP_{max} values. For each set of FRP_{min} and FRP_{max} values, the study area spatially explicit $FRE_{pwr.law}$ values were computed as described in section 4.6 and the medians of the 6539 Australia and the 245 Brazilian $FRE_{pwr.law}$ biomass burned estimates were derived. In this way, a total of 10,000 median $FRE_{pwr.law}$ and associated biomass burned estimates were obtained for each study area. The Brazilian sensitivity analysis was applied to the 4 day temporal duration thresholded FRP data as this threshold provided a median $FRE_{pwr.law}$ biomass burned estimate closest to the study area comparison (Table 3).

[43] Figure 13 shows the sensitivity analysis results for the Australian (Figure 13, left) and Brazilian (Figure 13, right) median FRE_{pwr} biomass burned estimates to the choice of FRP_{min} and FRP_{max} . The study area median $FRE_{pwr.law}$ biomass burned estimates are clearly sensitive to changes in FRP_{min} and FRP_{max} . The sensitivity is greatest

where the contours are most dense, occurring particularly when FRP_{min} is large and FRP_{max} is small. The Australian site is relatively less sensitive to FRP_{max} than FRP_{min} , which is always the case for $m > 2$. This can be inferred analytically from equation (8) as

$$\lim_{FRP_{max} \rightarrow \infty} FRE_{pwr.law} = d \frac{(m-1)}{(m-2)} FRP_{min}$$

when $m > 2$. In contrast for $m < 2$, as is the case for the Brazilian site, then FRE_{pwr} will depend on both FRP_{min} and FRP_{max} values.

[44] The Australian median biomass burned is less sensitive to changes in FRP_{max} than FRP_{min} ; the median biomass burned estimate changes by less than $\pm 20\%$ and up to $\pm 40\%$ when FRP_{max} and FRP_{min} are varied by $\pm 50\%$, respectively. The Brazilian median biomass burned estimate is about equally sensitive to changes in FRP_{min} and FRP_{max} , the median biomass burned estimate changes by slightly

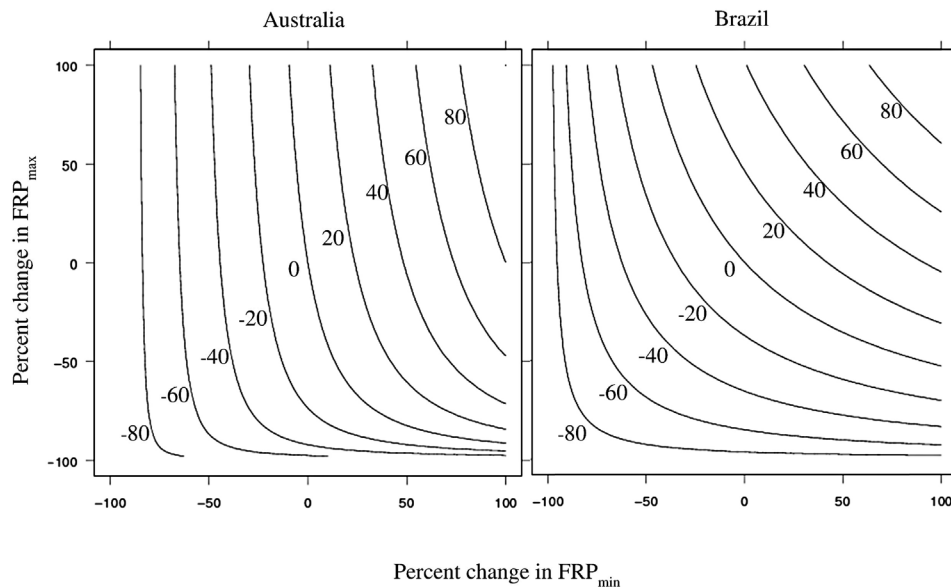


Figure 13. Sensitivity of the (left) Australian and (right) Brazilian median FRE_{pwr} biomass burned estimates to the choice of FRP_{min} and FRP_{max} . The contours show the relative percentage difference between the median biomass burned estimated using the observed study area FRP_{min} and FRP_{max} with respect to the median biomass burned estimated using simulated FRP_{min} and FRP_{max} values. The simulated FRP_{min} and FRP_{max} values were varied around the observed study area FRP_{min} and FRP_{max} values in 2% increments over a $\pm 100\%$ range.

more than $\pm 20\%$ when FRP_{\max} or FRP_{\min} are varied by $\pm 50\%$. These levels of biomass burned estimation sensitivity are relatively low or comparable to the likely errors found in landscape fuel load and combustion completeness information [Robinson, 1989; Ellicott et al., 2009; Vermote et al., 2009].

6. Discussion and Conclusions

[45] This paper has presented the theory and application of a new method to derive the fire radiative energy (FRE), and thus the biomass burned, from satellite fire radiative power (FRP) retrievals.

[46] The power law based FRE is derived as the product of the fire duration and the expected FRP. The latter is parameterized by the minimum and maximum FRP (FRP_{\min} and FRP_{\max}) and a scaling parameter (m) that is computed from the measured FRP data using a linear regression fit to probability distribution function in log scales methodology [Goldstein et al., 2004; Newman, 2005; Clauzet et al., 2009]. The sensitivity of the power law based FRE estimation method and the conventional temporal-integration-based FRE estimation method to FRP sampling was first quantified using FRP data retrieved from radiometer measurements of eight U.S. prescribed fires. The power law ($FRE_{\text{pwr.law}}$) and conventional temporal integration ($FRE_{\text{num.int}}$) FRE estimates were converted to total biomass burned using an established linear relationship [Wooster et al., 2005] and compared with the biomass burned measured independently as the difference in the prefire and postfire fuel loads. The $FRE_{\text{pwr.law}}$ - and conventional $FRE_{\text{num.int}}$ -derived biomass burned estimates were on average within 19.9% and 25.9%, respectively, of the eight measured estimates. The radiometer FRP data were then undersampled by randomly selecting without replacement 90%, 60%, 30%, and 15% of the FRP values for each fire. Both FRE estimation methods were sensitive to undersampling. If the power law parameters (m , FRP_{\min} , FRP_{\max}) were characterized a priori, from the original un-resampled FRP data, then the $FRE_{\text{pwr.law}}$ -derived biomass burned estimates were generally less sensitive to FRP undersampling than the conventional $FRE_{\text{num.int}}$ numerical integration method.

[47] One of the potential advantages of the new power law FRE estimation method is its inherent ability to compensate for (i) satellite FRP omission errors, due to undersampling caused by infrequent satellite overpasses and fire obscuration by clouds, smoke, and optically thick aerosols [Giglio, 2007; Roy et al., 2008]; and (ii) the decreased probability of satellite detection of fires with low FRP, due to factors including the changing size of the surface area sensed by the sensor detector, the variable relationship between fire front subpixel locations and the sensing system point spread function, the fire background characterization used by the FRP retrieval algorithm, and the presence of atmospheric water vapor [Wooster et al., 2005; Calle et al., 2009; Schroeder et al., 2010]. In this study, the FRP power law fit methodology was applied to MODIS FRP data by the use of a simple method to ignore low FRP values during the power law fit. The resulting power law fit was then applied to all FRP values to compensate for these effects.

[48] The conventional and power law based FRE estimation methodologies were applied to regional MODIS FRP data selected for Australian savanna and Brazilian forest study areas because they have contrasting fuel loads and burning conditions. The power law scaling parameter values (m) derived from the MODIS Terra and Aqua FRP data for the Australian and Brazilian fires had relative values that followed an expected pattern. A low m implies a greater proportion of high FRP fires, while a larger m implies a greater proportion of low FRP fires. The Brazilian m value (1.53) was lower than the Australian m value (2.14), which was expected because the Australian study area vegetation is predominantly spinifex grass that should burn less energetically than the Brazilian study area deforestation fires that have a higher fuel load and perhaps larger actively flaming fire fronts.

[49] For both the Australian and Brazilian study areas, MODIS FRE estimates were derived in a non-spatially explicit (a single estimate for the study area) and spatially explicit (different estimate for each active-fire detection pixel) manner [Boschetti and Roy, 2009]. The power law ($FRE_{\text{pwr.law}}$) and conventional temporal integration ($FRE_{\text{num.int}}$) FRE estimates were converted to total biomass burned estimates [Wooster et al., 2005] and compared with literature estimates. The Australian nonspatially explicit $FRE_{\text{num.int}}$ - and $FRE_{\text{pwr.law}}$ -based biomass burned results were comparable, about 81%, to the study area literature biomass burned value. The medians of the spatially explicit biomass burned estimates were 38% ($FRE_{\text{num.int}}$ based) and 60% ($FRE_{\text{pwr.law}}$ based) of the literature values. The Brazilian study area results were less comparable with the literature values. The Brazilian nonspatially explicit biomass estimates for either FRE estimation method yielded relatively poor results, most likely because the fires were not from the same progressively burning fire event that is implicitly assumed in the nonspatially explicit FRE computation [Boschetti and Roy, 2009]. The medians of the spatially explicit Brazilian burned biomass estimates were about 8% ($FRE_{\text{num.int}}$ -based) and 30% ($FRE_{\text{pwr.law}}$ -based) of the literature values, whereas the nonspatially explicit based biomass burned results were greater by a factor of about 3 ($FRE_{\text{num.int}}$) and 4.5 ($FRE_{\text{pwr.law}}$). We note, however, that the Brazilian study area literature burned biomass estimate we used may not be accurate, with reported standard errors of about 50% reported at a similar site [Balch et al., 2008].

[50] The power law method requires that the parameters of the FRP power law distribution (m , FRP_{\min} , FRP_{\max}) can be derived reliably from the FRP retrievals or that the parameters are known a priori. In the case of satellite FRP observations over large areas, it is reasonable to assume that the FRP probability distribution characteristics can be parameterized reliably a priori from fires over similar vegetation and with similar fire behavior [Freeborn et al., 2009]. Sensitivity analysis of the Australian and Brazilian MODIS FRP data indicate that the power law based FRE is sensitive to the selection of the FRP_{\min} and FRP_{\max} values in a nonlinear way that depends on the FRP distribution. However, a $\pm 50\%$ change in the FRP_{\min} or FRP_{\max} resulted in no more than a $\pm 40\%$ change in the burned biomass estimates. This level of sensitivity is relatively low or comparable to the errors found in traditional “bottom-up” biomass burned estimates based on fuel load and combustion completeness information

[Robinson, 1989; Ellicott et al., 2009; Vermote et al., 2009]. Over limited geographic areas it is likely that FRP_{\min} and FRP_{\max} derived from satellite FRP retrievals will not adequately capture the appropriate range of FRP. This fundamental issue requires further research and is complex because (i) the minimum and the maximum FRP detected by a satellite depends on the sensor characteristics, the active-fire detection algorithm, and the areal proportions and temperatures of the smoldering and flaming fire and nonburning components [Robinson, 1991; Giglio et al., 1999; Giglio and Justice, 2003; Ichoku et al., 2008], and (ii) the satellite overpass time should coincide with when the fire has minimum (e.g., started, or about to extinguish) and maximum (e.g., highest rate of combustion and maximum subpixel fire size) FRP.

[51] The power law FRE estimation method also requires fire duration information that can be derived by satellite active-fire detections through time, as implicitly assumed by conventional FRE estimation methods, or could be defined from other satellite products such as the MODIS burned area product that defines the approximate day of burning [Boschetti et al., 2010]. We recognize that, for the results reported in this study, the fire durations estimated from the MODIS active-fire detections may be biased by the necessary reprojection of MODIS swath (Level 2) to gridded (Level 3) data. This may increase the number of shorter duration fires or inflate the estimated durations that will have complex effects most notably on the spatially explicit (i.e., per pixel) FRE estimates.

[52] A rigorous validation of the results of this study would require the availability of FRE and biomass consumed over large areas, which are presently unavailable. The results and observations in this paper suggest, however, that the power law method of FRE estimation, exploiting the mathematical properties of probability distributions, opens a promising avenue for future research. Future research will be devoted to investigate whether the integration of multiple sources of data, for instance, polar-orbiting and geostationary FRP retrievals [Freeborn et al., 2009], could provide a regional depiction of the FRP power law distribution parameters. Future research will also investigate whether there is an explicit relationship between the scaling parameter m and the fire characteristics at regional scale, which would effectively allow the use of m to characterize fire behavior that is of interest to the ecological and the emissions modeling community but is difficult to determine over large areas using ground-based and satellite-based techniques [Wooster and Zhang, 2004; Roberts et al., 2009].

[53] **Acknowledgments.** The authors would like to thank the three anonymous reviewers for their insightful comments that helped greatly to refine the manuscript. This work was funded by NASA grants NNX07AF16G, NH08ZDA001N, and NNX10AN72H.

References

- Balch, J. K., D. C. Nepstad, P. M. Brando, L. M. Curran, O. Portela, O. De Carvalho, and P. Lefebvre (2008), Negative fire feedback in a transitional forest of southeastern Amazonia, *Global Change Biol.*, *14*(10), 2276–2287, doi:10.1111/j.1365-2486.2008.01655.x.
- Boschetti, L., and D. P. Roy (2009), Strategies for the fusion of satellite fire radiative power with burned area data for fire radiative energy derivation, *J. Geophys. Res.*, *114*, D20302, doi:10.1029/2008JD011645.
- Boschetti, L., D. P. Roy, C. O. Justice, and L. Giglio (2010), Global assessment of the temporal reporting accuracy and precision of the MODIS burned area product, *Int. J. Wildland Fire*, *19*(6), 705–709, doi:10.1071/WF09138.
- Calle, A., J.-L. Casanova, and F. González-Alonso (2009), Impact of point spread function of MSG-SEVIRI on active fire detection, *Int. J. Remote Sens.*, *30*(17), 4567–4579, doi:10.1080/01431160802609726.
- Carvalho, J. A., Jr., F. S. Costa, C. A. Gurgel Veras, D. V. Sandberg, E. C. Alvarado, R. Gielow, A. M. Serra Jr., and J. C. Santos (2001), Biomass fire consumption and carbon release rates of rainforest clearing experiments conducted in northern Mato Grosso, Brazil, *J. Geophys. Res.*, *106*, 17,877–17,887, doi:10.1029/2000JD900791.
- Chuvieco, E., and M. P. Martin (1994), Global fire mapping and fire danger estimation using AVHRR images, *Photogramm. Eng. Remote Sens.*, *60*, 563–570.
- Clauset, A., C. R. Shalizi, and M. E. J. Newman (2009), Power-law distributions in empirical data, *SIAM Rev.*, *51*(4), 661–703, doi:10.1137/070710111.
- Corral, A., L. Telesca, and R. Lasaponara (2008), Scaling and correlations in the dynamics of forest-fire occurrence, *Phys. Rev. E*, *77*(1), 016101, doi:10.1103/PhysRevE.77.016101.
- Crutzen, P. J., and M. O. Andreae (1990), Biomass burning in the tropics: Impact on atmospheric chemistry and biogeochemical cycles, *Science*, *250*(4988), 1669–1678, doi:10.1126/science.250.4988.1669.
- Daniels, A. (2007), *Field Guide to Infrared Systems*, SPIE, Bellingham, Wash.
- Denman, K. L., et al. (2007), Couplings between changes in the climate system and biogeochemistry, in *Climate Change 2007: The Physical Science Basis. Contribution of Working Group I to the Fourth Assessment Report of the Intergovernmental Panel on Climate Change*, edited by S. Solomon et al., Cambridge Univ. Press, New York.
- Downing, J. A., et al. (2006), The global abundance and size distribution of lakes, ponds, and impoundments, *Limnol. Oceanogr.*, *51*, 2388–2397.
- Ellicott, E., E. Vermote, L. Giglio, and G. Roberts (2009), Estimating biomass consumed from fire using MODIS FRE, *Geophys. Res. Lett.*, *36*, L13401, doi:10.1029/2009GL038581.
- Fernandes, R., and S. Leblanc (2005), Parametric (modified least squares) and non-parametric (Theil-Sen) linear regressions for predicting biophysical parameters in the presence of measurement errors, *Remote Sens. Environ.*, *95*(3), 303–316, doi:10.1016/j.rse.2005.01.005.
- Fredericksen, P. S., S. Langaas, and M. Mbaye (1990), NOAA-AVHRR and GIS-based monitoring of fire activity in Senegal—A provisional methodology and potential applications, in *Fire in the Tropical Biota: Ecosystem Processes and Global Challenges*, edited by J. G. Goldammer, pp. 400–417, Springer, Berlin.
- Freeborn, P. H., M. J. Wooster, W. M. Hao, C. A. Ryan, B. L. Nordgren, S. P. Baker, and C. Ichoku (2008), Relationships between energy release, fuel mass loss, and trace gas and aerosol emissions during laboratory biomass fires, *J. Geophys. Res.*, *113*, D01301, doi:10.1029/2007JD008679.
- Freeborn, P. H., M. J. Wooster, G. Roberts, B. D. Malamud, and W. Xu (2009), Development of a virtual active fire product for Africa through a synthesis of geostationary and polar orbiting satellite data, *Remote Sens. Environ.*, *113*(8), 1700–1711, doi:10.1016/j.rse.2009.03.013.
- Freeborn, P. H., M. J. Wooster, and G. Roberts (2011), Addressing the spatiotemporal sampling design of MODIS to provide estimates of the fire radiative energy emitted from Africa, *Remote Sens. Environ.*, *115*(2), 475–489, doi:10.1016/j.rse.2010.09.017.
- Fuller, D. O. (2000), Satellite remote sensing of biomass burning with optical and thermal sensors, *Prog. Phys. Geogr.*, *24*(4), 543–561.
- Giglio, L. (2007), Characterization of the tropical diurnal fire cycle using VIRS and MODIS observations, *Remote Sens. Environ.*, *108*(4), 407–421, doi:10.1016/j.rse.2006.11.018.
- Giglio, L., and C. O. Justice (2003), Effect of wavelength selection on characterization of fire size and temperature, *Int. J. Remote Sens.*, *24*(17), 3515–3520, doi:10.1080/0143116031000117056.
- Giglio, L., J. D. Kendall, and C. O. Justice (1999), Evaluation of global fire detection algorithms using simulated AVHRR infrared data, *Int. J. Remote Sens.*, *20*(10), 1947–1985, doi:10.1080/014311699212290.
- Giglio, L., J. Desclotres, C. O. Justice, and Y. J. Kaufman (2003), An enhanced contextual fire detection algorithm for MODIS, *Remote Sens. Environ.*, *87*(2–3), 273–282, doi:10.1016/S0034-4257(03)00184-6.
- Goldstein, M. L., S. A. Morris, and G. G. Yen (2004), Problems with fitting to the power-law distribution, *Eur. Phys. J. B.*, *41*(2), 255–258, doi:10.1140/epjb/e2004-00316-5.
- Ichoku, C., and Y. J. Kaufman (2005), A method to derive smoke emission rates from MODIS fire radiative energy measurements, *IEEE Trans. Geosci. Remote Sens.*, *43*(11), 2636–2649.
- Ichoku, C., L. Giglio, M. J. Wooster, and L. A. Remer (2008), Global characterization of biomass-burning patterns using satellite measurements of fire radiative energy, *Remote Sens. Environ.*, *112*(6), 2950–2962, doi:10.1016/j.rse.2008.02.009.

- Kaufman, Y. J., et al. (1996), Relationship between remotely sensed fire intensity and rate of emission of smoke: SCAR-C experiment, in *Global Biomass Burning*, edited by J. Levine, pp. 685–696, MIT Press, Cambridge, Mass.
- Kaufman, Y. J., C. O. Justice, L. P. Flynn, J. D. Kendall, E. M. Prins, L. Giglio, D. E. Ward, W. P. Menzel, and A. W. Setzer (1998), Potential global fire monitoring from EOS-MODIS, *J. Geophys. Res.*, *103*(D24), 32,215–32,238, doi:10.1029/98JD01644.
- Koren, I., L. Oreopoulos, G. Feingold, L. A. Remer, and O. Altaratz (2008), How small is a small cloud?, *Atmos. Chem. Phys. Discuss.*, *8*(2), 6379–6407, doi:10.5194/acpd-8-6379-2008.
- Korontzi, S., D. P. Roy, C. O. Justice, and D. E. Ward (2004), Modeling and sensitivity analysis of fire emissions in southern Africa during SAFARI 2000, *Remote Sens. Environ.*, *92*(3), 376–396, doi:10.1016/j.rse.2004.06.023.
- Kremens, R. L., A. M. S. Smith, and M. B. Dickinson (2010), Fire metrology: Current and future directions in physics-based measurements, *Fire Ecol.*, *6*, 13–35.
- Lentile, L. B., Z. A. Holden, A. M. S. Smith, M. J. Falkowski, A. T. Hudak, P. Morgan, S. A. Lewis, P. E. Gessler, and N. C. Benson (2006), Remote sensing techniques to assess active fire characteristics and post-fire effects, *Int. J. Wildland Fire*, *15*(3), 319–345, doi:10.1071/WF05097.
- Lin, J., and S. Rinaldi (2009), A derivation of the statistical characteristics of forest fires, *Ecol. Modell.*, *220*(7), 898–903, doi:10.1016/j.ecolmodel.2009.01.011.
- Loboda, T. V., and I. A. Csizsar (2007), Reconstruction of fire spread within wildland fire events in Northern Eurasia from the MODIS active fire product, *Global Planet. Change*, *56*(3–4), 258–273, doi:10.1016/j.gloplacha.2006.07.015.
- Malamud, B. D., J. D. A. Millington, and G. L. W. Perry (2005), Characterizing wildfire regimes in the United States, *Proc. Natl. Acad. Sci. U. S. A.*, *102*(13), 4694–4699, doi:10.1073/pnas.0500880102.
- Morton, D. C., R. S. Defries, J. T. Randerson, L. Giglio, W. Schroeder, and G. R. Van Der Werf (2008), Agricultural intensification increases deforestation fire activity in Amazonia, *Global Change Biol.*, *14*, 2262–2275, doi:10.1111/j.1365-2486.2008.01652.x.
- Mottram, G. N., M. J. Wooster, H. Balster, C. George, F. Gerrard, and J. Beisley (2005), The use of MODIS-derived fire radiative power to characterise Siberian boreal forest fires, paper presented at the 31st International Symposium on Remote Sensing of Environment, St. Petersburg, Russia.
- Newman, M. E. J. (2005), Power laws, Pareto distributions and Zipf's law, *Contemp. Phys.*, *46*(5), 323–351, doi:10.1080/00107510500052444.
- Riggan, P. J., R. G. Tissell, R. N. Lockwood, J. A. Brass, J. A. R. Pereira, H. S. Miranda, A. C. Miranda, T. Campos, and R. Higgins (2004), Remote measurements of energy and carbon flux from wildfires in Brazil, *Ecol. Appl.*, *14*(3), 855–872, doi:10.1890/02-5162.
- Roberts, G. J., and M. J. Wooster (2008), Fire Detection and Fire Characterization Over Africa Using Meteosat SEVIRI, *IEEE Trans. Geosci. Remote Sens.*, *46*(4), 1200–1218.
- Roberts, G. J., M. J. Wooster, G. L. W. Perry, N. Drake, L. M. Rebelo, and F. Dipotso (2005), Retrieval of biomass combustion rates and totals from fire radiative power observations: Application to southern Africa using geostationary SEVIRI imagery, *J. Geophys. Res.*, *110*, D21111, doi:10.1029/2005JD006018.
- Roberts, G., M. J. Wooster, and E. Lagoudakis (2009), Annual and diurnal African biomass burning temporal dynamics, *Biogeosciences*, *6*(5), 849–866, doi:10.5194/bg-6-849-2009.
- Robinson, J. M. (1989), On uncertainty in the computation of global emissions from biomass burning, *Clim. Change*, *14*(3), 243–261, doi:10.1007/BF00134965.
- Robinson, J. M. (1991), Fire from space—global fire evaluation using infrared remote-sensing, *Int. J. Remote Sens.*, *12*, 3–24, doi:10.1080/01431169108929628.
- Roy, D. P., L. Boschetti, C. O. Justice, and J. Ju (2008), The collection 5 MODIS burned area product—Global evaluation by comparison with the MODIS active fire product, *Remote Sens. Environ.*, *112*(9), 3690–3707, doi:10.1016/j.rse.2008.05.013.
- Russell-Smith, J., A. C. Edwards, and G. D. Cook (2003), Reliability of biomass burning estimates from savanna fires: Biomass burning in northern Australia during the 1999 Biomass Burning and Lightning Experiment B field campaign, *J. Geophys. Res.*, *108*(D3), 8405, doi:10.1029/2001JD000787.
- Saatchi, S. S., R. A. Houghton, R. C. Dos Santos, J. V. Soares, and Y. Yu (2007), Distribution of aboveground live biomass in the Amazon basin, *Global Change Biol.*, *13*, 816–837, doi:10.1111/j.1365-2486.2007.01323.x.
- Schroeder, W., E. Prins, L. Giglio, I. Csizsar, C. Schmidt, J. Morissette, and D. Morton (2008), Validation of GOES and MODIS active fire detection products using ASTER and ETM+ data, *Remote Sens. Environ.*, *112*(5), 2711–2726, doi:10.1016/j.rse.2008.01.005.
- Schroeder, W., I. Csizsar, L. Giglio, and C. C. Schmidt (2010), On the use of fire radiative power, area, and temperature estimates to characterize biomass burning via moderate to coarse spatial resolution remote sensing data in the Brazilian Amazon, *J. Geophys. Res.*, *115*, D21121, doi:10.1029/2009JD013769.
- Sen, P. K. (1968), Estimates of the regression coefficient based on Kendall's tau, *J. Am. Stat. Assoc.*, *63*, 1379–1389, doi:10.2307/2285891.
- Smith, A. M. S., and M. J. Wooster (2005), Remote classification of head and backfire types from MODIS fire radiative power and smoke plume observations, *Int. J. Wildland Fire*, *14*(3), 249–254, doi:10.1071/WF05012.
- Soares Neto, T. G., J. A. Carvalho Jr., C. A. G. Veras, E. C. Alvarado, R. Gielow, E. N. Lincoln, T. J. Christian, R. J. Yokelson, and J. C. Santos (2009), Biomass consumption and CO₂, CO and main hydrocarbon gas emissions in an Amazonian forest clearing fire, *Atmos. Environ.*, *43*(2), 438–446, doi:10.1016/j.atmosenv.2008.07.063.
- Song, W., J. Wang, K. Satoh, and W. Fan (2006), Three types of power-law distribution of forest fires in Japan, *Ecol. Modell.*, *196*(3–4), 527–532, doi:10.1016/j.ecolmodel.2006.02.033.
- Theil, H. (1950), A rank-invariant method of linear and polynomial regression analysis I, II and III, *Nederl. Akad. Wetensch. Proc.*, *53*, 386–392.
- van der Werf, G. R., J. T. Randerson, L. Giglio, G. J. Collatz, P. S. Kasibhatla, and A. F. Arellano Jr. (2006), Interannual variability in global biomass burning emissions from 1997 to 2004, *Atmos. Chem. Phys.*, *6*(11), 3423–3441, doi:10.5194/acp-6-3423-2006.
- van der Werf, G. R., D. C. Morton, R. S. DeFries, L. Giglio, J. T. Randerson, G. J. Collatz, and P. S. Kasibhatla (2008), Estimates of fire emissions from an active deforestation region in the southern Amazon based on satellite data and biogeochemical modelling, *Biogeosci. Discuss.*, *5*(4), 3533–3573, doi:10.5194/bgd-5-3533-2008.
- Vermote, E., E. Ellicott, O. Dubovik, T. Lapyonok, M. Chin, L. Giglio, and G. J. Roberts (2009), An approach to estimate global biomass burning emissions of organic and black carbon from MODIS fire radiative power, *J. Geophys. Res.*, *114*, D18205, doi:10.1029/2008JD011188.
- Wolfe, R. E., D. P. Roy, and E. Vermote (1998), MODIS land data storage, gridding, and compositing methodology: Level 2 grid, *IEEE Trans. Geosci. Remote Sens.*, *36*(4), 1324–1338.
- Wooster, M. J., and Y. H. Zhang (2004), Boreal forest fires burn less intensely in Russia than in North America, *Geophys. Res. Lett.*, *31*, L20505, doi:10.1029/2004GL020805.
- Wooster, M. J., G. Roberts, G. L. W. Perry, and Y. J. Kaufman (2005), Retrieval of biomass combustion rates and totals from fire radiative power observations: FRP derivation and calibration relationships between biomass consumption and fire radiative energy release, *J. Geophys. Res.*, *110*, D24311, doi:10.1029/2005JD006318.
- Zhang, B., F. W. Schwartz, and G. Liu (2009), Systematics in the size structure of prairie pothole lakes through drought and deluge, *Water Resour. Res.*, *45*, W04421, doi:10.1029/2008WR006878.
- Zinck, R. D., K. Johst, and V. Grimm (2010), Wildfire, landscape diversity and the Drossel-Schwabl model, *Ecol. Modell.*, *221*(1), 98–105, doi:10.1016/j.ecolmodel.2008.12.026.

L. Boschetti, Department of Geography, University of Maryland, 1113 LeFrak Hall, College Park, MD 20742, USA.

R. Kremens, Center for Imaging Science, Rochester Institute of Technology, 54 Lomb Memorial Dr., Rochester, NY 14623, USA.

S. S. Kumar and D. P. Roy, Geographic Information Science Center of Excellence, South Dakota State University, Brookings, SD 57007, USA. (david.roy@sdstate.edu)